Huntingtin interactome reveals huntingtin role in regulation of double strand break DNA damage response (DSB/DDR), chromatin remodeling and RNA processing pathways.

Tamara Ratovitski, [1*] Chloe D. Holland,[1] Robert N. O'Meally, [2]Alexey V. Shevelkin,[1] Tianze Shi,[1] Robert N. Cole,[2] Mali Jiang,[1] and Christopher A. Ross. [1,3*]

[1] Division of Neurobiology, Department of Psychiatry and Behavioral Sciences, Johns Hopkins University School of Medicine, 600 North Wolfe Street, CMSC 5 South, Baltimore, MD21287

[2] Mass Spectrometry and Proteomics Facility, Department of Biological Chemistry, Johns Hopkins University School of Medicine, 733 N. Broadway Street, Suite 371 BRB Baltimore, MD21287

[3] Departments of Neurology, Neuroscience and Pharmacology, Johns Hopkins University School of Medicine, Baltimore, MD21287

*Address correspondence to: Tamara Ratovitski (tratovi1@jhmi.edu) ORCHID ID 0000-0003-4020-5644 or Christopher A. Ross (caross@jhu.edu), CMSC 5 South, 600 North Wolfe Street, Baltimore, MD 21287. Phone: 410-614-0011

Running title

Huntingtin interactome in regulation of DNA repair

Abbreviations

Huntington's Disease (HD), huntingtin (HTT), DNA damage response (DDR), double strand break (DSB), nuclear speckles (NS), polyglutamine (polyQ), Non-Homologous End-Joining (NHEJ), RNA-binding proteins (RBPs), immortalized striatal precursor neurons (ISPN), medium spiny neurons (MSN) parallel reaction monitoring (PRM), post-translational modifications (PTMs), principal component analysis (PCA), protein-protein interaction (PPI), immunoprecipitation (IP), proximity ligation assay (PLA), low complexity regions (LCRs), intrinsically disordered regions (IDRs), endoplasmic reticulum (ER), adenosine triphosphate (ATP), wild type (WT), immunofluorescence (IF)

Keywords

Huntington's Disease, huntingtin, neurodegeneration, DNA damage, protein interactions, RNA processing, post-translational modifications

Conflicts of Interest:

The authors have no relevant financial or non-financial interests to disclose

Abstract

Huntington's Disease (HD), a progressive neurodegenerative disorder with no disease-modifying therapies, is caused by a CAG repeat expansion in the HD gene encoding polyglutamine-expanded huntingtin (HTT) protein. Mechanisms of HD cellular pathogenesis and cellular functions of the normal and mutant HTT proteins are still not completely understood. HTT protein has numerous interaction partners, and it likely provides a scaffold for assembly of multiprotein complexes many of which may be altered in HD. Previous studies have implicated DNA damage response in HD pathogenesis. Gene transcription and RNA processing has also emerged as molecular mechanisms associated with HD. Here we used multiple approaches to identify HTT interactors in the context of DNA damage stress. Our results indicate that HTT interacts with many proteins involved in the regulation of interconnected DNA repair/remodeling and RNA processing pathways. We present evidence for a role for HTT in double strand break repair mechanism. We demonstrate HTT functional interaction with a major DNA damage response kinase DNA-PKcs and association of both proteins with nuclear speckles. We show that S1181 phosphorylation of HTT is regulated by DSB, and can be carried out (at least *in vitro*) by DNA-PK. Furthermore, we show HTT interactions with RNA binding proteins associated with nuclear speckles, including two proteins encoded by genes at HD modifier loci, TCERG1 and MED15, and with chromatin remodeling complex BAF. These interactions of HTT may position it as an important scaffolding intermediary providing integrated regulation of gene expression and RNA processing in the context of DNA repair mechanisms.

Introduction

Huntington's Disease (HD) is a progressive neurodegenerative disorder with no disease-modifying therapies currently available (1-4). It is caused by a single mutation, CAG repeat expansion in the HD gene (*HTT*) and message (HTT), coding for expanded polyglutamine (polyQ) near the N-terminus of the mutant huntingtin (mHTT) protein (5). There is preferential degeneration of medium spiny neurons in the striatum, especially early in the disease course. HTT is a ~350 kDa protein with suggested scaffolding function (6), and numerous protein interactions, many of which are altered in HD (7-14).

Many studies have implicated HTT protein in the cellular DNA damage response (DDR) (15, 16), but most attention was concentrated on mismatch repair pathways since many of the loci for modifiers of HD age of onset code for proteins involved in DNA mismatch repair (FAN1, MSH2) (17-23). However, the gene products of mismatch-repair related genes have not emerged as HTT-interactors yet. Other studies suggest that HTT is involved in double strand break (DSB) repair mechanisms. Mutant HTT interacts with Ku70, an essential DSB repair protein and a regulatory component of the DNA-dependent protein kinase (DNA-PK) (24, 25). HTT was found at DNA damage sites co-localizing with another major DSB-induced kinase, ATM (ataxia telangiectasia mutated) (26), and targeting ATM ameliorated mutant Huntingtin toxicity (27). HTT has also been implicated in transcription-coupled (TC) DNA DSB repair coordinating a chromatin remodeler BRG1(SMARCA4) -dependent TC Non-Homologous End-Joining (TC-NHEJ) complex to repair DSB in neurons (16, 28, 29).

RNA processing has also emerged as a molecular mechanism associated with HD, based on several expression profiling, RNA-seq and proteomics studies in HD models (11, 13, 30-35). Our previous methyl-proteome analysis has identified a cluster of RNA-binding splicing factors interacting with HTT (35). Many RNA-binding proteins (RBPs), including those interacting with HTT, have been recently implicated in the DDR (36-42). HTT role in chromatin remodeling via its interaction and facilitation of polycomb repressive complex (PRC2) have been suggested (43), While there are many reports of HTT-interacting proteins , to our knowledge there has not been systematic investigation of HTT interactome under conditions of DNA-damage stress.

Recent studies from the McCarroll lab, combining CAG repeat sizing with RNA-seq in the same individual cells, have suggested that somatic expansion to very long repeat lengths is central to HD pathogenesis (44-46). They showed that Medium Spiny Neurons (MSN) with up to 150

CAG repeats have surprisingly few changes in gene expression, while neurons with greater than 150 CAGs have loss of important MSN-appropriate, cell-type-defining messages and inappropriate expression of messages related to development or cell toxicity. Our immortalized striatal precursor neurons (ISPN) HD model (with 180 CAG and expanding) (47) is uniquely suited to study interactions of HTT protein with very long repeats as most relevant to HD pathogenesis.

Using ISPN model, we now find that DSB repair response is impaired in HD neurons and that HTT phosphorylation at S1181 site is regulated by the induction of DSBs. We show that phospho-HTT interacts with DNA-PKcs (catalytic subunit of DNA-PK complex) and that both proteins co-localize to nuclear speckles (NS), essential subnuclear organelles involved in all steps of RNA processing. In addition, we found HTT interaction with components of chromatin remodeling complex BAF.

Our analyses of HTT interactome using both an affinity purification and a novel proximity-based approach supports the function of HTT in the regulation of translation, RNA metabolism, chromatin remodeling and DSB repair (distinct from mismatch repair), suggesting potential role of HTT in facilitating interplay and emerging interconnections between these pathways.

Results

DSB repair response is impaired in HD immortalized striatal precursor neurons (*ISPNs).*

One of the earliest consequences of activation of DDR kinases (ATM, DNA-PK and ATR) at DSBs is phosphorylation of the histone variant H2A.X on serine (S139) producing γH2AX which is a key step in signaling and initiating the repair of DSBs. After the initial phosphorylation of H2A.X at sites flanking DSBs, numerous DSB repair proteins are recruited resulting in further activation of ATM and phosphorylation of H2A.X histones, forming γH2A.X foci that are easily detected by immunofluorescence-based assays (48). Thus, γH2A.X is a sensitive molecular marker of both DNA damage and repair (49).

We sought to evaluate DSB repair response in HD neurons by measuring and quantifying γ-H2A.X foci that are formed in our immortalized striatal precursor neurons (ISPNs) (47) undergoing DDR. ISPNs are human patient-derived iPSCs differentiated to a striatal precursor stage, and then immortalized. DSB/DDR was induced by treatment with bleomycin (5-10μg/ml, 30min) which led to activation of γ-H2A.X and p-ATM as shown by immunoblotting (**Fig. 1A**). γ-H2A.X foci were visualized by immunofluorescence (IF) with γ-H2A.X specific antibody (**Fig.**

1B). As described before (50), we observed small foci formed at the early stages of the DDR, decreasing in number and increasing in size as the DDR progressed. It has been suggested that when the number of DSBs exceeds the cellular capacity, γH2A.X is visualized as "apoptotic ring" or diffuse halos rather than distinct foci, and these are associated with apoptosis and not with DSB. (50). We observed such pan-nuclear γH2A.X staining in about 5-10% of the cells (**Fig. S1**), and these were excluded from analysis.

We employed a 3D-visualization and quantitation using Imaris software. Nuclei were chosen as a region of interest for individual cells and 3D surface was constructed using "DAPI" channel for quantitation of nuclear γ-H2A.X foci. Our analysis shows significantly lower γH2A.X foci size and intensity in HD ISPNs compared to control (**Fig. 1C**), consistent with a deficiency of HD ISPNs in mounting an adequate DSB repair response. HD ISPNs demonstrate more vulnerability to DSB induced (by bleomycin) cellular stress compared to normal neurons (**Fig. 1D**), as shown by decreased viability (ATP) and increased apoptosis (activation of caspase 3/7).

Phosphorylated huntingtin participates in DSB/DDR via interaction with components of nuclear speckles (NS)

Post-translational modifications (PTMs) are major regulators of protein function and interactions. Several PTMs of HTT have been found to modulate HTT biochemical properties and expanded HTT toxicity (6, 51-57). We sought to investigate if the stoichiometry of HTT phosphorylation at specific sites is affected by bleomycin-induced DNA damage, thus suggesting a role for these modifications in the regulation of DSB/DDR pathways in HD. Using parallel reaction monitoring (PRM) we quantified by mass spectrometry the relative stoichiometry of phosphorylation sites in HTT from control and HD ISPNs with and without bleomycin treatment. We targeted the most prominent phosphorylation sites previously identified in various systems (57). Phosphorylation at S421, S1201, S1876 and S2114/2116 sites was significantly increased in 180CAG ISPNs compared to control cells in both stressed and non-stressed conditions (**Fig. S2**). The stoichiometry of phosphorylation at one site, S1181, was dramatically increased in HD cells upon bleomycin treatment (**Fig. 2A**) suggesting potential role of this PTM in DSB response in HD ISPNs.

To further investigate the details of subcellular localization of pS1181-HTT we employed IF with pS1181 specific antibody (57) followed by confocal microscopy (**Fig. 2B**). We observed localization of endogenous pS1181 HTT within the nuclear compartment, forming nuclear puncta.

3D-visualization and quantitation analysis (Imaris) showed significantly increased volume and intensity of these puncta in HD ISPNs after induction of DSB, compared to normal ISPNs (**Fig. 2C**). Notably, pS1181 HTT puncta did not co-localize with γH2A-X foci in control or HD ISPNs (**Fig. 2B**) and were also negative for other subnuclear markers: nucleolin (nucleoli), coilin (Cajal bodies) and PML (PML nuclear bodies) (data not shown). Instead, we found a striking co-localization with nuclear speckles (NS) marker SC35 /SRSF2 (**Fig. 3A, B**). NS are subnuclear organelles involved in all aspects of RNA processing (58). As assessed by 3D quantitation (**Fig. 3C**), organization of SC35 into nuclear speckles was altered in HD cells. Intensity, density, and total volume of SC35-positive nuclear speckles increased upon induction of DSB in normal ISPNs. By contrast, these measures were decreased or not changed in HD cells. NS positive for both phospho-HTT and SC35 appeared disorganized and completely disintegrated in a proportion of HD ISPNs with a few large speckles formed in some cells (indicated by arrows on **Fig. 3A**).

We sought to test whether HTT may interact with other proteins associated with NS in our ISPN system. We targeted TCERG1 (Transcription elongation regulator1), a coilin-associated factor essential for Cajal body formation and integrity, and snRNP biogenesis (59). The TCERG1 locus is also a genetic modifier for HD (59, 60) and TCERG1 protein has previously been reported to interact with HTT (61, 62) and to co-localize with NS marker SC35 (63). To confirm endogenous interaction of HTT with TCERG1, we conducted co-IPs in our ISPN model (**Fig. S3-B**). Total cell lysates were prepared from control (33) and HD (180) ISPNs treated with bleomycin (10μg/ml, 2h) and untreated (NT), and HTT complexes were immuno-precipitated using antibodies to total HTT (MCA2050). We observed TCERG1/HTT co-localization in the nuclei (**Fig. S3-A**). Proximity Ligation Assay (PLA) demonstrated decreased interaction in HD cells (**Fig. S3-C, D**).

Unbiased screen for HTT interactors upon induction of DSB/DDR

Diminished DSB response observed in HD neurons, and HTT interaction with a major RNA-processing organelle (NS) prompted us to explore how HTT may be involved in the regulation of interconnected DNA damage response and RNA-processing pathways. We conducted an unbiased HTT interactome screen in ISPNs differentiated into medium-spiny-neuron-like cultures (as described previously), undergoing genotoxic stress. Differentiated ISPNs (47) recapitulate major HD-related phenotypes of the parental iPSC model, including brain-derived neurotrophic factor (BDNF)-withdrawal-induced cell death that can be rescued by small molecules previously validated in the parental iPSCs (7, 8, 13). After induction of DSBs with bleomycin

(10μg/ml, 30min) HTT protein complexes were pulled down from normal (33CAG) and HD (180CAG) neurons using a mixture of anti-HTT antibodies (MCA2050 and 2051) followed by quantitative mass spectrometry (TMT-based) to compare the relative protein abundances in the pulldowns. Three samples were analyzed for each condition. 499 proteins have been identified with at least 2 unique peptides and quantified (471 with high confidence 1% FDR) in all six HTT immunoprecipitates. Protein abundances were normalized by HTT protein abundance to account for variability between individual HTT pulldowns. Out of these proteins, 333 decreased >20% in abundance in HD ISPNs (HD/Cont <0.8), while 40 increased by >20% (HD/Cont >1.2). Biological replicates of two groups of cells were well separated by the principal component analysis (PCA) based on normalized protein abundances (generated using PD2.4, **Fig. 4A**). The hierarchical clustering heat map (**Fig. 4B**) and Volcano plots (**Fig. 4C**) demonstrate that majority of proteins were less abundant in the pulldowns from HD neurons.

We focused on proteins found less abundant in the pulldowns from HD ISPNs (relative to control cells) and performed pathway and process enrichment analysis using "Metascape" analysis tools (64). This dataset was significantly and highly enriched in biological processes associated with protein translation and RNA metabolism (mRNA splicing and micro-RNA biogenesis, **Fig. 4D**). Protein-protein Interaction (PPI) enrichment analysis (Metacsape) identified protein networks with best-scoring terms by p-value with functional description of the corresponding networks shown in the tables below (**Fig. 4E**). Networks involved in translation, chromatin remodeling and RNA processing have been identified with the highest enrichment p-value suggesting potential dysregulation of these pathways due to weakened or partially lost interactions in HD neurons. These results are consistent with previous expression profiling, RNA-seq and proteomics studies in HD models implicating RNA biogenesis, processing, splicing and gene expression in HD pathogenesis (11, 13, 30-33).

HTT is phosphorylated by and co-localizes and interacts with DNA-PKcs

We targeted one of the proteins with decreased abundance in HD ISPNs pulldowns (HD/Cont =0.64, **Fig. 5A**), DNA-PKcs (PRKDC), a catalytic subunit of an essential DSB repair complex DNA-dependent protein kinase (DNA-PK). DNA-PK is central in the process of Non-Homologous End Joining (NHEJ), which is the main DSB repair pathway used by neurons (reviewed in (16, 48, 65). Mutant HTT has been previously shown to interact with Ku70 (24, 25),

a regulatory component of this complex required for recruitment and activation of DNA-PKcs (66).

We confirmed endogenous interaction of HTT with DNA-PKcs using co-immunoprecipitations (co-IP) in our ISPN model (**Fig. 5B**). Total cell lysates were prepared from control (33) and HD (180) ISPNs treated with bleomycin (10μg/ml, 2h) and untreated (NT), and HTT complexes were immuno-precipitated using antibodies to total HTT (MCA2050, two top panels). DNA-PKcs and HTT were detected in the immunoprecipitates (IPs). Notably, an antibody to DNA-PKcs was able to pulldown pS1181-HTT from ISPNs in the co-IP assay (middle panels), suggesting potential interaction (**Fig. 5B**).

We asked whether DNA-PK can phosphorylate HTT. *In vitro* phosphorylation assays were conducted with recombinant HTT-23Q/HAP40 complex (purified by Curia as described in Methods). Recombinant DNA-PK complex (purified from HeLa cells, Promega), activated by the addition of linear double-stranded DNA, was incubated with HTT/HAP40 for indicated times, and phosphorylation state of HTT was assessed using phospho-specific antibodies to four phosphorylation sites on HTT (previously described in (57). We observed a significant increase in S1181 phosphorylation (normalized to total HTT), but not at other sites analyzed (**Fig. 5C**).

We found partial co-localization of DNA-PKcs with pS1181-HTT nuclear puncta using IF and confocal microscopy (**Fig. 5D**). PLA confirmed proximity (suggesting direct interaction) of endogenous pS1181-HTT and DNA-PKcs (**Fig. 5E**). We observed a dramatic increase in PLA sites concentrating in the nucleus of normal ISPNs after induction of DSBs by bleomycin. Significantly less PLA signals were detected in HD cells with a decrease in the number and intensity in the nucleus upon bleomycin treatment. These observations are consistent with disrupted interactions between DNA-PKcs and HTT in HD cells with potential implications for DSB repair processes.

DNA-PKcs is autophosphorylated at multiple sites (67). Phosphorylation at S2056 (within PRQ cluster) is induced by DSB (68) but is not required for DNA-PK activation (69, 70). We observed an increase in DNA-PKcs phosphorylation (S2056) in normal ISPNs (33CAG) upon induction of DSB with bleomycin (**Fig. 6A**). The levels of pDNA-PKcs in HD ISPNs (180CAG) were dramatically decreased with no induction by DSB, suggestive of dysregulation of at least some processes within DSB repair pathways.

pDNA-PKcs was previously found to accumulate at nuclear speckles (NS) outside of DNA damage sites at late time points upon DSB induction suggesting a role for DNA-PK in the regulation of alternative splicing during genotoxic stress (71). In our ISPN model we also observed accumulation of pDNA-PKcs at SC35-positive nuclear speckles 2h upon induction of DSB (**Fig. 6 B**). It is particularly intriguing because we also found co-localization of phospho-HTT (pS1181) to NS (**Fig. 3**).

Huntingtin (HTT) interacts with BAF chromatin remodeling complex and with Mediator complex

Transcription and chromatin remodeling were the most prominent highly enriched categories among the proteins that increased in abundance in HD ISPNs (based on FC>1.2) which may suggest a stronger interaction with expanded HTT. Metascape PPI enrichment analysis identified two protein complexes of particular interest **(Fig. 7A):** first- comprising most of the components of BAF chromatin remodeling complex, and second- including five subunits of transcriptional Mediator complex, including MED15, whose locus is genetic modifier for HD found in a recent GWAS study (72). We aimed to further characterize HTT interactions with components of BAF chromatin remodeling complex closely related to DNA repair.

To confirm endogenous interaction of HTT with BAF complex identified in MS experiments, we conducted co-IPs in our ISPN model (**Fig. 7B**). Total cell lysates were prepared from control (33) and HD (180) ISPNs treated with bleomycin (10μg/ml, 2h) and untreated (NT), and HTT complexes were immuno-precipitated using antibodies to total HTT (MCA2050). We targeted two components of BAF complex- BRG1 (SMARCA4) and ARID1A, which were detected in the IPs with specific antibodies.

IF with confocal microscopy showed partial co-localization of HTT with BRG1 and ARID1A (**Fig. 8A and 9A**). Endogenous interaction of HTT with BRG1 and ARID1A was confirmed by PLA (**Fig. 8B and 9B**). We observed robust PLA signals in the nuclei of both un-treated and bleomycin-treated normal (33CAG) ISPNs. A dramatic decrease in PLA sites number and intensity was recorded in HD ISPNs with some induction upon bleomycin treatment for BRG1/HTT PLA signals. These observations are consistent with disrupted interactions between BAF complex and nuclear HTT in HD cells. Using 3D quantification (Imaris) we previously found that HD ISPNs showed lower HTT-immunoreactivity in the nucleus (Ratovitski 2022). As illustrated on **Fig S4**, we observed decreased nuclear presence of HTT in most HD ISPNs and increased HTT localization to perinuclear structures positive for Golgi marker, GM130 (**Fig. S4**),

which may partially account for decreased nuclear PLA signals for BRG1/HTT and ARID1A/HTT proximity.

Ascorbate peroxidase (APEX2) -mediated proximity-based proteomics for HTT protein interactions

Most of the previous HTT interactome studies have used HTT affinity purifications (HTT pulldowns) followed by mass spectrometry. However, such co-IP experiments performed on cell lysates after disruption of cellular structures may capture complexes formed in solution in addition to endogenous interactions. These methods are highly dependent on the antibodies to the bait protein which may introduce additional bias. Proximity-based proteomics provides several advantages compared to traditional approaches to study protein interactions including yeast two-hybrid systems and affinity purifications. Ascorbate peroxidase (APEX2) -based proximity labeling (with APEX2-tagging) can detect weak or dynamic interactions and can preserve the intracellular spatial information of the interactomes since during tagging, cells are still alive, membranes are intact, and protein complexes are undisrupted. Furthermore, the temporal changes of the HTT interactome in response to acute cellular stresses cannot be easily resolved using traditional approaches. APEX2 enzyme mediates biotinylation of proteins located in its proximity in living cells. TMT-mediated proteomics workflow can be performed after enrichment for biotinylated peptides to quantify potential interactors. To our knowledge, only one HTT interactome study using proximity proteomics have been reported (73).

To test the APEX2-labeling approach we have generated APEX2- fusion constructs with full-length WT (23Q) and polyQ-expanded (82Q) HTT (4 samples for each group were analyzed). Biotin-labeling was performed as described (74) and conditions were optimized to ensure sufficient biotinylation, enrichment, and reduction of non-specific binding (**Figure S5**). No biotin (lane 2) was added for negative control. Biotinylated proteins were enriched by streptavidin pulldown and detected in the inputs and in the eluted samples (but not in negative controls). Fewer biotinylated proteins in flow-through indicates of efficient binding to streptavidin resin.

To increase the specificity of the assay we have modified previously published protocol (73, 74) and performed trypsin digestion of the lysates first, followed by enrichment for biotinylated peptides, instead of a pulldown of biotinylated proteins (which may include proteins non-specifically binding to streptavidin resin) (see Methods for details). 82% (1315 out of 1603) of peptide groups identified using this approach contained biotin- tyramide modfication,

representing 356 proteins. Raw protein abundances were normalized to APEX2 protein (within Protein Discoverer workflow) and used to calculate the protein level ratios to negative control (no biotin added). 250 proteins, found in all samples, showed sample/negative control ratios of at least 10. We selected this group of proteins found in proximity of HTT (and thus potential HTT-interactors) to perform pathway and process enrichment analysis using "Metascape" tools (64).

The most enriched GO terms in this dataset were metabolism of RNA, and regulation of translation as well as protein folding and stress response **(Fig. 10 A).** Protein-protein Interaction (PPI) enrichment analysis (**Fig. 10B**, Metacsape) identified networks involved in metabolism and transport of RNA, translation, protein localization to chromatin and protein folding with the highest enrichment p-value.

Using this approach in transfected HEK293 cells we found minimal differences between WT (23Q) and expanded (82Q) HTT interactomes. We detected 16 HTT peptides with biotin-tyramide modifications, which may be a result of intramolecular proximity of the N-terminal APEX2 tag on HTT to its other domains. In addition, endogenous WT HTT may come close and form complexes with transfected APEX2-tagged HTT-82Q, thus producing a background of biotinylated proteins that are proximal to both mutant transfected and endogenous WT HTT. Because 'biotinylation radius' is not a fixed value the endogenous proteins that are many nanometers away from APEX2 may still be biotinylated, although weakly, and detected by MS. This background may account for minimal differences between APEX2-tagged HTT interactomes. To overcome this difficulty it would be beneficial to engineer APEX2 tag on the endogenous HTT (e.g. by CRISPR) in the future studies. APEX2 tag can also be placed at the C-terminus or within other portions of HTT to further explore domain-specific interactions.

Discussion

We used multiple approaches to reveal HTT protein interactions in the context of DNA damage response including novel proximity-based methods which can preserve the intracellular spatial information of the interactomes. Our analyses of HTT interactome using both an affinity purification and proximity-based approach supports the role of HTT in the regulation of interconnected DNA repair/remodeling and RNA processing pathways.

Phospho-HTT is implicated in protein interactions described in this study. There is solid support in the literature for the role of PTMs in HTT functionality and perhaps in mutant HTT

toxicity. (6, 54). Enzymes catalyzing some of these modifications have been suggested as potential therapeutic targets (51-53, 55, 56, 75). We have previously identified several dozen phosphorylation, acetylation and arginine methylation/dimethylation sites from HD knock-in mice, human post-mortem brain and immortalized striatal precursor neurons, and defined their effects on HTT solubility and toxicity (14, 52, 57).

We show here that S1181 phosphorylation is regulated by DSB and can be carried out (at least *in vitro*) by a major DSB kinase DNA-PK. This is particularly intriguing because we found both phospho-HTT and DNA-PKcs proteins co-localizing with NS. Association of HTT with SC35-positive speckles was first noticed two decades ago (76). HTT phosphorylated at the N-terminal sites was localized to SC35 positive speckles upon oxidative stress (77). In another recent study (78) phospho-N17-HTT was found to co-localize with both SC35-positive nuclear speckles and NEAT1 paraspeckles. In this study we found that HTT phosphorylated at the previously characterized S1181 site (51, 52, 57, 75) forms nuclear puncta co-localizing with NS marker SC35 (SRSF2).

As previously suggested (71), pDNA-PKcs localized to NS may participate in the regulation of alternative splicing during genotoxic stress. HTT/DNA-PKcs interaction and localization of both pDNA-PKcs and pS1181-HTT proteins to NS is indicative of potential functional cooperation in regulation of RNA processing. Liu et al (71) found that DNA-PK inactivation affects splicing of a set of pre-mRNAs, including major splicing regulators SRSF1 and SRSF2. Notably, both splicing factors have been shown to be mis-spliced in HD (31, 33).

Autophosphorylation of DNA-PKcs at PQR cluster (which includes S2056) participates in DNA end-processing and the pathway choice for DSB repair (69, 79). Several studies reported that phosphorylation at this site is not required for activation of DNA-PKcs and it has been suggested to facilitate the dissociation of DNA-PKcs from DNA ends at damage sites (69, 70, 80). Considering that S2056 can be phosphorylated in response to ionizing radiation that induce DSB, (68), it can be used a measure of an active DNA repair, or a completion of such and dissociation of DNA-PKcs from the complex. We found a dramatic decrease of pDNA-PKcs protein level in HD ISPNs with no induction by DSB, suggestive of dysregulation of DSB repair processes.

Although NS have been primarily associated with RNA splicing and storing of multiple splicing factors, they also harbor proteins crucial for epigenetic regulation, chromatin organization, transcription and DNA repair (58). Furthermore, an extensive biochemical study (81) demonstrated

a stable association of NS with chromatin. Spatial proximity to NS was shown to directly correlate with amplification of gene expression (reviewed in (82). In this model transcriptional activation is boosted by NS which deliver RNA-processing factors to the nascent RNAs. Thus, NS may play a direct role in facilitating integrated regulation of gene expression.

Examples of RBPs, also HTT-interactors (35), found in NS, include FUS, EWSR1, and HNRNPUL1. Transcription-related factors - TCERG1 and components of the Mediator complex were also found associated with NS (63, 83). Recent study (84) suggests a link between the Mediator complex and NS, with Med15, a subunit in the tail module of the Mediator complex, forming nuclear condensates. BAF complex subunits have been shown to interact with splicing factors or other proteins localized to NS, such as RNA polymerase II (85) suggesting a mechanism where chromatin remodeling at specific genes could influence RNA splicing. Two other current studies (preprints) (29, 86) report HTT interaction with both BAF and Mediator complexes in mouse brain and SH-SY5Y cell model. Thus, interaction of HTT with TCERG1, Mediator complex and chromatin remodelers, that we found in this study, may occur at least in part in NS, facilitating communication between transcription and RNA splicing.

In our co-IP /mass spectrometry study we found higher abundances of the subunits of BAF complex, BRG1 and ARID1A, in HTT pulldowns from HD ISPNs, which may indicate of increased interaction. However, using a proximity-based method (PLA), which can preserve the intracellular spatial information of the interactomes, we found a reduction in the nuclear PLA signals between HTT and subunits of BAF complex in HD ISPNs, suggesting loss of functional nuclear interactions, mediated in part by the depletion of HTT in the nuclei of HD neurons.

Proteins containing low complexity regions (LCRs), generally corresponding to intrinsically disordered regions (IDRs) are over-represented in NS proteins. Such proteins, including HTT (14, 87), are prone to phase-separation in the conditions of cellular crowding, which is considered a major force maintaining the integrity of NS lacking lipid membranes. Several studies demonstrated NS morphology changes following transcriptional inhibition and genotoxic stress (81, 88). Kim et al confirmed liquid state properties of NS and tracked the motion and fusion of speckles into bigger and increased intensity droplets after transcriptional inhibition or stress responses. This was attributed to splicing factors diffusing back into speckles from active transcription sites. We found that NS appeared disorganized in HD ISPNs with a few large speckles formed in some cells, which would be consistent with an increased stress burden in HD ISPNs

exacerbated by the induction of DNA damage. Decreased viability of HD cells upon ER and oxidative stress have been demonstrated (77, 89). Here we show an increased vulnerability of HD patient-derived neurons to genotoxic stress including reduced viability (ATP) and increased apoptosis (activation of caspase 3/7) after induction of DSB by bleomycin.

Many splicing factors found in NS are modified post-translationally and these PTMs within their LCRs may regulate their protein interactions, function and association with NS. We showed previously that HTT interacts with PRMTs enzymes (protein arginine methyl transferases) and affect their activity (14). Arginine methylation, a modification that plays a major role in the function of RBPs (reviewed in (90, 91), was decreased for several NS proteins in HD neurons (35). Here we found that HTT can also interact with DNA-PKcs, a major DDR kinase that has numerous substrates not only among DNA repair proteins, but also among RBPs, such as FUS which is phosphorylated by DNA-PK following DNA damage and binds DSB (37). Thus, mutant HTT may alter RNA processing and transcription via abnormal interactions with modifying enzymes (PRMTs, kinases) and other DDR proteins involved in the maintenance of genome stability.

Conclusions

Our study highlights the role of HTT in the emerging integration and interplay between DDR/DNA remodeling and RNA processing pathways (reviewed in (40, 92, 93) mediated in part by DDR kinases regulating RNA metabolism in response to DNA damage. The activation of the DDR can modify RNA splicing by affecting expression and modifications of various transcription, splicing, and mRNA export proteins (92). Several DDR proteins and RBPs have a dual function in RNA processing and DNA repair and may be directly involved in the prevention and repair of DNA lesions (40). Chromatin remodeling is also closely related to DNA repair: DDR kinases regulate the chromatin and nucleosome rearrangements near a DSB to provide a scaffold for the recruitment of other DDR factors and inhibit local transcription. DDR-dependent H2A.X phosphorylation induces changes to chromatin structure by recruiting ATP-dependent chromatin remodeling complexes including SWI/SNF (48). Thus, genotoxic stress affects chromatin remodeling and RNA splicing activity via modification and reengagement of splicing factors and other mechanisms, while nuclear speckles emerge as multifunctional organelles providing an integrated regulation of gene expression and RNA processing.

We suggest that HTT functional interactions with modifying enzymes (such as DDR kinase DNA-PK and PRMTs), its association with NS, with numerous RBPs, and with chromatin remodeler BAF may position HTT as a unique scaffolding intermediary providing interconnections among these pathways. Recent data (94) indicate that mHTT ribotoxicity extends beyond translation of mHTT itself, and that accumulating mHTT protein fragments sequester eIF5A leading to progressive, age-dependent depletion of eIF5A in HD cells and mouse brains. Previous HTT interactome studies (10-12) revealed HTT involvement with other cytoplasmic processes such as actin cytoskeleton regulation, axonal transport vesicular trafficking and chaperone-mediated stress response. Our data presented here, as well as other current findings highlight nuclear mechanisms such as chromatin remodeling, transcription and splicing. Thus HTT may be in a central position for regulation of multiple cellular accommodations to DNA damage stress. Further characterization of the functional consequences of these interactions will help elucidate the impact of HTT-lowering therapy and may provide important insight into HD pathogenesis and therapeutic targets.

Methods

Cells

Immortalized Striatal Precursor Neurons (ISPNs) were generated in our laboratory from patient-derived iPS cells with normal (33) or expanded (180) CAG repeats using co-expression of the enzymatic component of telomerase hTERT and drug regulated c-Myc. as described previously (47). Notably, our 180CAG HD ISPN line has been undergoing CAG repeat expansion and the CAG size at the time of these studies ranged from 240 to 260. For clarity, we are refferring to this line as 180CAG throughout this paper. The ISPNs were propagated as stable adherent neuronal precursors using Matrigel-coated plates with SCM2 medium (47) at 37ºC and 5% CO_2. Differentiation to a phenotype resembling Medium Spiny Neurons was performed as previously described (47). Human embryonic kidney (HEK) 293FT cells were obtained from Invitrogen (ThermoFisher) and were grown in DMEM (with 4.5 g/L D-Glucose, ThermoFisher) supplemented with 10% FBS, 100 µg/ml Geneticin, 100 units/ml penicillin and 100 units/ml streptomycin.

Cell viability/apoptosis assays

For cell viability/apoptosis assays, 1 x 10^4 ISPN cells / well were plated in Matrigel coated 96 well plates. 24 hours after plating, adenosine triphosphate (ATP) levels were measured using CellTiter-Glo® Luminescent Cell Viability Assay (Promega) in triplicate wells for each condition. Each individual well was assumed as biological replicate for statistical analysis. For cell apoptosis assay we used Caspase-Glo® 3/7 Assay System (Promega).

HTT in vitro phosphorylation assay

HTT/HAP40 complex purification was conducted by Curia. HAP40 was added as stabilizing binding partner (95). Baculoviruses expressing C-terminal FLAG-tagged HTT-23Q and N-terminal myc-tagged HAP40 were produced, and HEK293 cells were transduced with both viruses. HTT-HAP40 complexes were isolated using FLAG affinity purification. The following buffers were used: Cell Lysis buffer- 50 mM Tris pH8, 300 mM NaCl, 10% glycerol, 5 mM EDTA, protease inhibitors; Wash buffer-50 mM Tris pH8, 300 mM NaCl, 10% glycerol, 10% glycerol, 0.01% Tween 20; Elution buffer-50 mM Tris pH8, 300 mM NaCl, 10% glycerol, 0.5% CHAPS, 0.4 mg/mL FLAG peptide.

In vitro phosphorylation assays were carried out with DNA-PK (Promega, #V581A) according to the manufacturer's protocol. 200units of DNA-PK complex, activated by addition of 10 μg/ml of calf thymus DNA, was mixed with 5ug of purified HTT/HAP40 complex for indicated times, and phosphorylation state of HTT was assessed using phospho-specific antibodies to S1181, S1201, S1864, and S2116 (57).

IP and western blotting

For detection of endogenous HTT the following antibodies were used: MCA2050 (HDB4E10, Bio-Rad) directed to amino acids 1844-2131 of HTT, MCA2051 (HDC8A4, Bio-Rad) directed to amino acids 2703-2911of HTT, and MW1 anti- polyQ (Developmental Studies Hybridoma Bank, University of Iowa) to detect mutant HTT in HD ISPNs. Antibodies to phospho-HTT (S1181, S1201, S1864, S2116) were previously described (57). Other antibodies used: ATM [2C1] from Genetex (#GTX70103); phospho-ATM (Ser1981) from R&D Systems (#AF1655); phospho-histone H2A.X (S139) [3F2] from Genetex (#GTX80694); histone H2A.X (D17A3) from Cell Signaling Technology (#7631); phospho DNA- PKcs (S2056) from Abcam (#18192); DNA-PKcs [E6U3A] from Cell Signaling Technology (#38168); TCERG1/CA150 from Bethyl Laboratories (#A300-360A); BRG1[BLR106H] from Bethyl Laboratories (#A700-106);

ARID1A/BAF250 [BLR279L] from Bethyl Laboratories (#A700-279); b-actin [C4] from Santa Cruz Biothechnology (#sc-47778).

For detection of HTT interactions by co-immunoprecipitation ISPN cells were collected and lysed in co-IP buffer [50mM Tris, 150mM NaCl, 5mM EDTA, 50mM MgCl2, 0.5% Triton, 0.5% Sodium deoxycholate] in the presence of protease inhibitors (PIC, Protease Inhibitor Cocktail III, Calbiochem) and Halt™ Phosphatase Inhibitor Cocktail (ThermoFisher) followed by centrifugation at 14,000g. The resulting supernatants were diluted 1:1 with PBS and were pre-cleared by incubation with protein G- agarose for 1h at 4^0C. IPs were carried out ON at 4^0C using either antibodies to HTT (1:1 mix of MCA2050 and MCA2051) or to protein-specific antibodies (described above). The IPs were washed 3 times with the lysis buffer, and protein complexes were eluted from the beads with 2xSDS Laemmli sample buffer (Bio-Rad), fractionated on SDS-PAGE and detected by western blotting with antibodies described above. Inputs were collected prior to IP to control for protein levels.

Quantitation of the stoichiometry of phosphorylation sites on HTT

Quantitative targeted parallel reaction monitoring (PRM) mass spectrometry was performed for modified peptides chosen from previous discovery data dependent acquisitions (DDA) and was carried out as described previously (14).

Unbiased screen for HTT interactors upon induction of DSB/DDR

Normal (33CAG) and HD (180CAG) ISPNs were differentiated into medium-spiny-neuron-like cultures and DSBs were induced with bleomycin (10μg/ml, 30min). HTT protein complexes were pulled down using a mixture of anti-HTT antibodies (MCA2050 and 2051) as described above except elution from the beads was performed using 1% SDS/PBS buffer. The relative abundance of co-precipitating with HTT proteins from 3 control (33) and 3 HD (180) cell lysates were compared using isobaric mass tags (Tandem Mass Tags, TMT 6-plex, ThermH2A.XFisher Scientific) with nanoflow reverse-phase liquid chromatography tandem mass spectrometry (RP-nLCMS/MS) as previously described (35).

Briefly, samples were reduced with dithiothreitol and alkylated with iodoacetamide, then digested with trypsin overnight at 37C, acidified with TFA, and desalted on a Waters Oasis HLB 96 well plate (30mg) prior to Isobaric Mass labeling (TMT). TMT labeling was performed according to manufacturer recommendations. TMT-labeled peptides were fractionated on a 1mm x 10 cm XBridge C18 Column.

Peptides were analyzed on an Orbitrap-Fusion Lumos mass spectrometer (ThermoFisher Scientific) interfaced with an Easy-nLC1200 UPLC by reversed-phase chromatography Survey scans (MS) of precursor ions were acquired from 350-1400 m/z at 120,000 resolution. Precursor ions were isolated with a 0.7 m/z window by data dependent monitoring over 3 seconds and a 15s dynamic exclusion. Peptides were fragmented using an HCD activation collision energy 38, an AGC of 1e5, and a maximum injection time of 100ms at 50,000 resolution.

Fragmentation spectra were processed by Proteome Discoverer v2.4 (PD2.4, ThermoFisher Scientific) and searched with Mascot v.2.6.2 (Matrix Science, London, UK) against RefSeq v.83 Human database. Search criteria: trypsin as the enzyme, one allowed missed cleavage, 5 ppm precursor mass tolerance, 0.02 Da fragment mass tolerance. Modifications included: TMT 6Plex on N-terminus, carbamidomethylation on C as static, TMT 6Plex on K, oxidation on M, deamidation on N or Q. Peptide identifications from the Mascot searches were processed within PD2.4 using Percolator at a 5% False Discovery Rate confidence threshold, based on an auto-concatenated decoy database search. Peptide spectral matches (PSMs) were filtered for Isolation Interference <30%. Relative protein abundances of identified proteins were determined in PD2.4 from the normalized median ratio of TMT reporter ions. The data were normalized by HTT abundance by Proteome Discoverer (PD2.4) to compensate for minor differences between individual HTT pulldowns). Technical variation in ratios from our mass spectrometry analysis is less than 10% (96).

APEX2-mediated proximity labeling for HTT interactions

FL-HTT-23Q and polyQ-expanded, FL-HTT-82Q plasmids encoding untagged full length HTT were described previously (57). APEX2-HTT N-terminal fusions were generated by GenScript. HEK293 cells were transfected with APEX2-HTT-23Q and APEX2-HTT-82Q plasmids (using Lipofectamine 2000, Invitrogen) and APEX2-mediated labeling was performed 24h after transfection as previously described (73, 74). Briefly, 500 µM biotinyl tyramide (biotin phenol) (Tocris; #6241) in Dulbecco's modified Eagle's medium (ThermoFisher) supplemented with 10% fetal bovine serum and 1% penicillin/streptomycin was added to all experimental plates except for negative control plates. Labeling was initiated after 1 hour by adding H2O2 (1 mM final concentration) for 1 min to all plates. The labeling reaction was quenched by aspirating media from the plate and immediately rinsing three times with the quenching solution: 5 mM trolox ((+/−)-6-hydroxy-2,5,7,8-tetramethylchromane- 2-carboxylic acid, (Sigma #238813]), 10 mM

sodium L-ascorbate (Sigma, #A4034), and 10 mM sodium azide in PBS supplemented with protease inhibitors (PIC, Protease Inhibitor Cocktail III, Calbiochem). Cells were then incubated on ice in fresh quenching solution 3 times for 5 min each. Following the last wash cells were lysed in RIPA buffer (50 mM Tris pH7, 150 mM NaCl, 0.1% SDS, 0.5% sodium deoxycholate, 1% Triton X-100) supplemented with protease inhibitors, 10mM sodium azide, 10mM sodium ascorbate, and 5 mM Trolox.

200 µl (~200µg of protein) of cell lysate per sample were reduced, alkylated, digested with trypsin and desalted as described above, and subsequently dried in a speed vacuum. Dried peptides were solubilized in RIPA buffer and incubated with 300 µl Pierce™ magnetic streptavidin beads (Thermofisher) overnight at 4° to enrich for biotinylated peptides. After incubation, the beads were washed sequentially with the following buffers to remove nonspecific proteins: twice with RIPA buffer, once with 1 M KCl, once with 0.1 M Na2CO3, twice with RIPA buffer and twice with PBS. After the last wash, biotinylated peptides were eluted from streptavidin beads by incubation with 600 µl of neat hexafluoroisopropanol (HFIP) for 5 min at RT. After second elution the supernatants were combined into one tube and then dried in a speed vacuum. The dried peptides were processed for mass spectrometry following TMT labeling as described above.

Fragmentation spectra were processed by Proteome Discoverer v2.4 (PD2.4, ThermoFisher Scientific) and searched as above with Mascot v.2.6.2 (Matrix Science, London, UK) against RefSeq v.83 Human database including custom APEX2 sequence (L-ascorbate peroxidase APx2 Q39843_SOYBN). Modifications included as above, plus biotin tyramide. The data were normalized by the abundance of APEX2 protein by Proteome Discoverer (PD2.4)

Graphs and Pathway and Process Enrichment Analysis:

PCA plots, Heat map and Volcano plots were built by PD2.4 using normalized abundances of proteins. Pathway and Process Enrichment Analyses were performed using “Metascape” (64). Protein-protein Interaction (PPI) Enrichment Analyses were generated by “Metacsape” using following databases: STRING6, BioGrid7, OmniPath8, InWeb_IM9. Only physical interactions in STRING (physical score > 0.132) and BioGrid were used. The resultant networks contain the subset of proteins that form physical interactions with at least one other member in the list. If the network contains between 3 and 500 proteins, the Molecular Complex Detection (MCODE) algorithm10 has been applied to identify densely connected network components. Pathway and process enrichment analysis has been applied to each MCODE component independently, and the

best-scoring terms by p-value have been retained as the functional description of the corresponding components, shown in the tables underneath corresponding network plots within Figures 4 and 10.

Immunofluorescence (IF) and proximity ligation assay (PLA)

Immunofluorescence (IF) was carried out using standard methods after the fixation of the cells with 4% PFA. Cells were permeabilized with 0.1% Triton-X100 for 10 min, blocked with 5% goat serum and incubated with primary antibodies ON at 4^0C. The following primary antibodies were used for staining: phospho-histone H2A.X (S139) [3F2, mouse] from Genetex (#GTX80694); phospho-histone H2A.X (S139) [20E3, rabbit mAb] from Cell Signaling Technology (#60566); phospho-DNA PKcs (S2056) from Abcam (#18192); DNA-PKcs [3H6, mouse] from Cell Signaling Technology (#12311); SC35 [SC-35] from Sigma-Aldrich (#S4045); TCERG1/CA150 from Invitrogen (#PA5-84824); BRG1 [A52] from Cell Signaling Technology (#3508); ARID1A [EPR13501] from Abcam(#182560); MCA2050 and S1181 (described above) for HTT. Secondary antibodies: goat anti-rabbit IgG Alexa Fluor 488 and goat anti-mouse IgG Alexa Fluor 555 (ThermoFisher). Images were acquired with Zeiss LSM 710 confocal microscopes (Carl Zeiss Microscopy, LLC, White Plains, NY).

We performed quantitation of γ-H2A.X foci, and of nuclear puncta positive for pS1181-HTT or for SC35 using Imaris (Bitplane AG, Zurich, Switzerland) and Huygens Essential (Scientific Volume Imaging B.V., Netherlands, www.svi.nl) software. The confocal parameters were determined, and the same settings were applied for each sample within the dataset. The images with z-stacks were collected using Zen image collection software (Carl Zeiss Microscopy) and processed for 3D reconstruction. For correct measurement of colocalization, preliminary image deconvolution was performed to eliminate background and noise of fluorescent signal. We have chosen a region of interest for individual cells and made a 3D surface of nucleus using "DAPI" channel. Analysis was performed on five images per group (taken from independent wells) with 7-12 cells per image.

PLA was performed using Duolink® In Situ Mouse/Rabbit kit (Millipore Sigma) according to the manufacturer's protocol and using primary antibodies described above. PLA signals were quantitated using MetaXpress software (Molecular Devices). Number of PLA sites per cell, sum intensity of PLA sites per cell and average PLA site intensity were reported relative to technical negative control within a given experiment. 3-4 images were taken from independent wells; a total of 30-50 cells were analyzed for each condition.

Statistical Analysis

Statistical analysis was performed using SigmaPlot software. The data was first checked using Shapiro-Wilk normality test and equal variance test. If passed, t-test with equal variances was performed for two groups comparisons. If normality or equal variance test failed- Mann-Whitney Rank Sum Test was performed. For multiple group comparisons we used One Way Analysis of Variance (ANOVA) with pairwise multiple comparison procedures (Holm-Sidak method). Graphs showing individual experimental values were built using Prism (GraphPad). In the experiments involving cell imaging each individual plate/well was assumed as biological replicate. In the experiments involving evaluation of protein expression each individual experiment was assumed as biological replicate. The statistical tests used in each figure, number of biological replicates for each assay, and all P values for statistically significant results are noted in the Figure Legends.

Data availability

All data is available from the corresponding authors upon reasonable request.

Acknowledgements

This work was supported by National Institutes of Health: 5R21NS109412-02 to T.R., 5R01NS08645208 to C.A.R., and by the JHU HD Precision Medicine Center of Excellence (CHDI). We thank Tom Vogt for discussions.

References

1 Bates, G.P., Dorsey, R., Gusella, J.F., Hayden, M.R., Kay, C., Leavitt, B.R., Nance, M., Ross, C.A., Scahill, R.I., Wetzel, R. *et al.* (2015) Huntington disease. *Nat Rev Dis Primers*, **1**, 15005.

2 Ross, C.A., Aylward, E.H., Wild, E.J., Langbehn, D.R., Long, J.D., Warner, J.H., Scahill, R.I., Leavitt, B.R., Stout, J.C., Paulsen, J.S. *et al.* (2014) Huntington disease: natural history, biomarkers and prospects for therapeutics. *Nat Rev Neurol*, **10**, 204-216.

3 Ross, C.A. and Tabrizi, S.J. (2011) Huntington's disease: from molecular pathogenesis to clinical treatment. *Lancet Neurol*, **10**, 83-98.

4 Tabrizi, S.J., Flower, M.D., Ross, C.A. and Wild, E.J. (2020) Huntington disease: new insights into molecular pathogenesis and therapeutic opportunities. *Nat Rev Neurol*, **16**, 529-546.

5 The Huntington's Disease Collaborative Research Group (1993) A novel gene containing a trinucleotide repeat that is expanded and unstable on Huntington's disease chromosomes. The Huntington's Disease Collaborative Research Group. *Cell*, **72**, 971-983.

6 Saudou, F. and Humbert, S. (2016) The Biology of Huntingtin. *Neuron*, **89**, 910-926.

7 Kedaigle, A.J., Fraenkel, E., Atwal, R.S., Wu, M., Gusella, J.F., MacDonald, M.E., Kaye, J.A., Finkbeiner, S., Mattis, V.B., Tom, C.M. *et al*.(2020) Bioenergetic deficits in Huntington's disease iPSC-derived neural cells and rescue with glycolytic metabolites. *Hum Mol Genet*, **29**, 1757-1771

8 Consortium, H.D.i. (2017) Developmental alterations in Huntington's disease neural cells and pharmacological rescue in cells and mice. *Nat Neurosci*, **20**, 648-660.

9 Greco, T.M., Secker, C., Ramos, E.S., Federspiel, J.D., Liu, J.P., Perez, A.M., Al-Ramahi, I., Cantle, J.P., Carroll, J.B., Botas, J. *et al.* (2022) Dynamics of huntingtin protein interactions in the striatum identifies candidate modifiers of Huntington disease. *Cell Syst*, **13**, 304-320 e305.

10 Harjes, P. and Wanker, E.E. (2003) The hunt for huntingtin function: interaction partners tell many different stories. *Trends Biochem Sci*, **28**, 425-433.

11 Ratovitski, T., Chighladze, E., Arbez, N., Boronina, T., Herbrich, S., Cole, R.N. and Ross, C.A. (2012) Huntingtin protein interactions altered by polyglutamine expansion as determined by quantitative proteomic analysis. *Cell Cycle*, **11**, 2006-2021.

12 Li, S.H. and Li, X.J. (2004) Huntingtin-protein interactions and the pathogenesis of Huntington's disease. *Trends Genet*, **20**, 146-154.

13 HD iPSC Consortium (2012) Induced pluripotent stem cells from patients with Huntington's disease show CAG-repeat-expansion-associated phenotypes. *Cell Stem Cell*, **11**, 264-278.

14 Ratovitski, T., Jiang, M., O'Meally, R.N., Rauniyar, P., Chighladze, E., Farago, A., Kamath, S.V., Jin, J., Shevelkin, A.V., Cole, R.N. *et al.* (2022) Interaction of huntingtin with PRMTs and its subsequent arginine methylation affects HTT solubility, phase transition behavior and neuronal toxicity. *Hum Mol Genet*, **31**, 1651-1672.

15 Maiuri, T., Bowie, L.E. and Truant, R. (2019) DNA Repair Signaling of Huntingtin: The Next Link Between Late-Onset Neurodegenerative Disease and Oxidative DNA Damage. *DNA Cell Biol*, **38**, 1-6.

16 Pradhan, S., Gao, R., Bush, K., Zhang, N., Wairkar, Y.P. and Sarkar, P.S. (2022) Polyglutamine Expansion in Huntingtin and Mechanism of DNA Damage Repair Defects in Huntington's Disease. *Front Cell Neurosci*, **16**, 837576.

17 Genetic Modifiers of Huntington's Disease, C. (2015) Identification of Genetic Factors that Modify Clinical Onset of Huntington's Disease. *Cell*, **162**, 516-526.

18 Genetic Modifiers of Huntington's Disease Consortium. Electronic address, g.h.m.h.e. and Genetic Modifiers of Huntington's Disease, C. (2019) CAG Repeat Not Polyglutamine Length Determines Timing of Huntington's Disease Onset. *Cell*, **178**, 887-900 e814.

19 Goold, R., Hamilton, J., Menneteau, T., Flower, M., Bunting, E.L., Aldous, S.G., Porro, A., Vicente, J.R., Allen, N.D., Wilkinson, H. *et al.* (2021) FAN1 controls mismatch repair complex assembly via MLH1 retention to stabilize CAG repeat expansion in Huntington's disease. *Cell Rep*, **36**, 109649.

20 Iyer, R.R. and Pluciennik, A. (2021) DNA Mismatch Repair and its Role in Huntington's Disease. *J Huntingtons Dis*, **10**, 75-94.

21 McAllister, T.E., England, K.S., Hopkinson, R.J., Brennan, P.E., Kawamura, A. and Schofield, C.J. (2016) Recent Progress in Histone Demethylase Inhibitors. *J Med Chem*, **59**, 1308-1329.

22 Moss, D.J.H., Pardinas, A.F., Langbehn, D., Lo, K., Leavitt, B.R., Roos, R., Durr, A., Mead, S., investigators, T.-H., investigators, R. *et al.* (2017) Identification of genetic variants associated with Huntington's disease progression: a genome-wide association study. *Lancet Neurol*, **16**, 701-711.

23 Pinto, R.M., Dragileva, E., Kirby, A., Lloret, A., Lopez, E., St Claire, J., Panigrahi, G.B., Hou, C., Holloway, K., Gillis, T. *et al.* (2013) Mismatch repair genes Mlh1 and Mlh3 modify CAG instability in Huntington's disease mice: genome-wide and candidate approaches. *PLoS Genet*, **9**, e1003930.

24 Enokido, Y., Tamura, T., Ito, H., Arumughan, A., Komuro, A., Shiwaku, H., Sone, M., Foulle, R., Sawada, H., Ishiguro, H. *et al.* (2010) Mutant huntingtin impairs Ku70-mediated DNA repair. *J Cell Biol*, **189**, 425-443.

25 Tamura, T., Sone, M., Iwatsubo, T., Tagawa, K., Wanker, E.E. and Okazawa, H. (2011) Ku70 alleviates neurodegeneration in Drosophila models of Huntington's disease. *PLoS One*, **6**, e27408.

26 Maiuri, T., Mocle, A.J., Hung, C.L., Xia, J., van Roon-Mom, W.M. and Truant, R. (2017) Huntingtin is a scaffolding protein in the ATM oxidative DNA damage response complex. *Hum Mol Genet*, **26**, 395-406.

27 Lu, X.H., Mattis, V.B., Wang, N., Al-Ramahi, I., van den Berg, N., Fratantoni, S.A., Waldvogel, H., Greiner, E., Osmand, A., Elzein, K. *et al.* (2014) Targeting ATM ameliorates mutant Huntingtin toxicity in cell and animal models of Huntington's disease. *Sci Transl Med*, **6**, 268ra178.

28 Gao, R., Chakraborty, A., Geater, C., Pradhan, S., Gordon, K.L., Snowden, J., Yuan, S., Dickey, A.S., Choudhary, S., Ashizawa, T. *et al.* (2019) Mutant huntingtin impairs PNKP and ATXN3, disrupting DNA repair and transcription. *Elife*, **8**.

29 Pradhan, S., Bush, K., Zhang, N., Pandita, R.K., Tsai, C.L., Smith, C., Pandlebury, D.F., Gaikwad, S., Leonard, F., Nie, L. *et al.* (2024) Chromatin remodeler BRG1 recruits huntingtin to repair DNA double-strand breaks in neurons. *bioRxiv*, in press.

30 Elorza, A., Marquez, Y., Cabrera, J.R., Sanchez-Trincado, J.L., Santos-Galindo, M., Hernandez, I.H., Pico, S., Diaz-Hernandez, J.I., Garcia-Escudero, R., Irimia, M. *et al.* (2021) Huntington's disease-specific mis-splicing unveils key effector genes and altered splicing factors. *Brain*, **144**, 2009-2023.

31 Lin, L., Park, J.W., Ramachandran, S., Zhang, Y., Tseng, Y.T., Shen, S., Waldvogel, H.J., Curtis, M.A., Faull, R.L., Troncoso, J.C. *et al.* (2016) Transcriptome sequencing reveals aberrant alternative splicing in Huntington's disease. *Hum Mol Genet*, **25**, 3454-3466.

32 Ratovitski, T., Chaerkady, R., Kammers, K., Stewart, J.C., Zavala, A., Pletnikova, O., Troncoso, J.C., Rudnicki, D.D., Margolis, R.L., Cole, R.N. *et al.* (2016) Quantitative Proteomic Analysis Reveals Similarities between Huntington's Disease (HD) and Huntington's Disease-Like 2 (HDL2) Human Brains. *J Proteome Res*, **15**, 3266-3283.

33 Tano, V., Utami, K.H., Yusof, N., Begin, J., Tan, W.W.L., Pouladi, M.A. and Langley, S.R. (2023) Widespread dysregulation of mRNA splicing implicates RNA processing in the development and progression of Huntington's disease. *EBioMedicine*, **94**, 104720.

34 Xing, Y., Wang, R. and Davidson, B.L. (2022) Mis-splicing in Huntington's disease: harnessing the power of comparative transcriptomics. *Trends Neurosci*, **45**, 91-93.

35 Ratovitski, T., Kamath, S.V., O'Meally, R.N., Gosala, K., Holland, C.D., Jiang, M., Cole, R.N. and Ross, C.A. (2023) Arginine methylation of RNA-binding proteins is impaired in Huntington's disease. *Hum Mol Genet*, **32**, 3006-3025.

36 Britton, S., Dernoncourt, E., Delteil, C., Froment, C., Schiltz, O., Salles, B., Frit, P. and Calsou, P. (2014) DNA damage triggers SAF-A and RNA biogenesis factors exclusion from chromatin coupled to R-loops removal. *Nucleic Acids Res*, **42**, 9047-9062.

37 Deng, Q., Holler, C.J., Taylor, G., Hudson, K.F., Watkins, W., Gearing, M., Ito, D., Murray, M.E., Dickson, D.W., Seyfried, N.T. *et al.* (2014) FUS is phosphorylated by DNA-PK and accumulates in the cytoplasm after DNA damage. *J Neurosci*, **34**, 7802-7813.

38 Gurunathan, G., Yu, Z., Coulombe, Y., Masson, J.Y. and Richard, S. (2015) Arginine methylation of hnRNPUL1 regulates interaction with NBS1 and recruitment to sites of DNA damage. *Sci Rep*, **5**, 10475.

39 Levone, B.R., Lenzken, S.C., Antonaci, M., Maiser, A., Rapp, A., Conte, F., Reber, S., Mechtersheimer, J., Ronchi, A.E., Muhlemann, O. *et al.* (2021) FUS-dependent liquid-liquid phase separation is important for DNA repair initiation. *J Cell Biol*, **220**.

40 Mikolaskova, B., Jurcik, M., Cipakova, I., Kretova, M., Chovanec, M. and Cipak, L. (2018) Maintenance of genome stability: the unifying role of interconnections between the DNA damage response and RNA-processing pathways. *Curr Genet*, **64**, 971-983.

41 Polo, S.E., Blackford, A.N., Chapman, J.R., Baskcomb, L., Gravel, S., Rusch, A., Thomas, A., Blundred, R., Smith, P., Kzhyshkowska, J. *et al.* (2012) Regulation of DNA-end resection by hnRNPU-like proteins promotes DNA double-strand break signaling and repair. *Mol Cell*, **45**, 505-516.

42 Wang, W.Y., Pan, L., Su, S.C., Quinn, E.J., Sasaki, M., Jimenez, J.C., Mackenzie, I.R., Huang, E.J. and Tsai, L.H. (2013) Interaction of FUS and HDAC1 regulates DNA damage response and repair in neurons. *Nat Neurosci*, **16**, 1383-1391.

43 Seong, I.S., Woda, J.M., Song, J.J., Lloret, A., Abeyrathne, P.D., Woo, C.J., Gregory, G., Lee, J.M., Wheeler, V.C., Walz, T. *et al.* (2010) Huntingtin facilitates polycomb repressive complex 2. *Hum Mol Genet*, **19**, 573-583.

44 Handsaker, R.E., Kashin, S., Reed, N.M., Tan, S., Lee, W.-S., McDonald, T.M., Morris, K., Kamitaki, N., Mullally, C.D., Morakabati, N. *et al.* (2024) Long somatic DNA-repeat expansion drives neurodegeneration in Huntington disease. *bioRxiv*, in press., 2024.2005.2017.592722.

45 Matlik, K., Baffuto, M., Kus, L., Deshmukh, A.L., Davis, D.A., Paul, M.R., Carroll, T.S., Caron, M.C., Masson, J.Y., Pearson, C.E. *et al.* (2024) Cell-type-specific CAG repeat expansions and toxicity of mutant Huntingtin in human striatum and cerebellum. *Nat Genet*, **56**, 383-394.

46 Pressl, C., Matlik, K., Kus, L., Darnell, P., Luo, J.D., Paul, M.R., Weiss, A.R., Liguore, W., Carroll, T.S., Davis, D.A. *et al.* (2024) Selective vulnerability of layer 5a corticostriatal neurons in Huntington's disease. *Neuron*, **112**, 924-941 e910.

47 Akimov, S.S., Jiang, M., Kedaigle, A.J., Arbez, N., Marque, L.O., Eddings, C.R., Ranum, P.T., Whelan, E., Tang, A., Wang, R. *et al.* (2021) Immortalized striatal precursor neurons from Huntington's disease patient-derived iPS cells as a platform for target identification and screening for experimental therapeutics. *Hum Mol Genet*, **30**, 2469-2487.

48 Sirbu, B.M. and Cortez, D. (2013) DNA damage response: three levels of DNA repair regulation. *Cold Spring Harb Perspect Biol*, **5**, a012724.

49 Mah, L.J., El-Osta, A. and Karagiannis, T.C. (2010) gammaH2AX: a sensitive molecular marker of DNA damage and repair. *Leukemia*, **24**, 679-686.

50 Solier, S. and Pommier, Y. (2014) The nuclear gamma-H2AX apoptotic ring: implications for cancers and autoimmune diseases. *Cell Mol Life Sci*, **71**, 2289-2297.

51 Anne, S.L., Saudou, F. and Humbert, S. (2007) Phosphorylation of huntingtin by cyclin-dependent kinase 5 is induced by DNA damage and regulates wild-type and mutant huntingtin toxicity in neurons. *J Neurosci*, **27**, 7318-7328.

52 Arbez, N., Ratovitski, T., Roby, E., Chighladze, E., Stewart, J.C., Ren, M., Wang, X., Lavery, D.J. and Ross, C.A. (2017) Post-translational modifications clustering within proteolytic domains decrease mutant huntingtin toxicity. *J Biol Chem*, **292**, 19238-19249.

53 Colin, E., Zala, D., Liot, G., Rangone, H., Borrell-Pages, M., Li, X.J., Saudou, F. and Humbert, S. (2008) Huntingtin phosphorylation acts as a molecular switch for anterograde/retrograde transport in neurons. *EMBO J*, **27**, 2124-2134.

54 Ehrnhoefer, D.E., Sutton, L. and Hayden, M.R. (2011) Small changes, big impact: posttranslational modifications and function of huntingtin in Huntington disease. *Neuroscientist*, **17**, 475-492.

55 Gu, X., Greiner, E.R., Mishra, R., Kodali, R., Osmand, A., Finkbeiner, S., Steffan, J.S., Thompson, L.M., Wetzel, R. and Yang, X.W. (2009) Serines 13 and 16 are critical determinants of full-length human mutant huntingtin induced disease pathogenesis in HD mice. *Neuron*, **64**, 828-840.

56 Jiang, M., Zhang, X., Liu, H., LeBron, J., Alexandris, A., Peng, Q., Gu, H., Yang, F., Li, Y., Wang, R. *et al.* (2020) Nemo-like kinase reduces mutant huntingtin levels and mitigates Huntington's disease. *Hum Mol Genet*, **29**, 1340-1352.

57 Ratovitski, T., O'Meally, R.N., Jiang, M., Chaerkady, R., Chighladze, E., Stewart, J.C., Wang, X., Arbez, N., Roby, E., Alexandris, A. *et al.* (2017) Post-Translational Modifications (PTMs), Identified on Endogenous Huntingtin, Cluster within Proteolytic Domains between HEAT Repeats. *J Proteome Res*, **16**, 2692-2708.

58 Galganski, L., Urbanek, M.O. and Krzyzosiak, W.J. (2017) Nuclear speckles: molecular organization, biological function and role in disease. *Nucleic Acids Res*, **45**, 10350-10368.

59 Moreno-Castro, C., Prieto-Sanchez, S., Sanchez-Hernandez, N., Hernandez-Munain, C. and Sune, C. (2019) Role for the splicing factor TCERG1 in Cajal body integrity and snRNP assembly. *J Cell Sci*, **132**.

60 Lobanov, S.V., McAllister, B., McDade-Kumar, M., Landwehrmeyer, G.B., Orth, M., Rosser, A.E., network, R.I.o.t.E.H.s.d., Paulsen, J.S., Group, P.-H.I.o.t.H.S., Lee, J.M. *et al.* (2022) Huntington's disease age at motor onset is modified by the tandem hexamer repeat in TCERG1. *NPJ Genom Med*, **7**, 53.

61 Holbert, S., Denghien, I., Kiechle, T., Rosenblatt, A., Wellington, C., Hayden, M.R., Margolis, R.L., Ross, C.A., Dausset, J., Ferrante, R.J. *et al.* (2001) The Gln-Ala repeat transcriptional activator CA150 interacts with huntingtin: neuropathologic and genetic evidence for a role in Huntington's disease pathogenesis. *Proc Natl Acad Sci U S A*, **98**, 1811-1816.

62 Tourette, C., Li, B., Bell, R., O'Hare, S., Kaltenbach, L.S., Mooney, S.D. and Hughes, R.E. (2014) A large scale Huntingtin protein interaction network implicates Rho GTPase signaling pathways in Huntington disease. *J Biol Chem*, **289**, 6709-6726.

63 Sanchez-Alvarez, M., Goldstrohm, A.C., Garcia-Blanco, M.A. and Sune, C. (2006) Human transcription elongation factor CA150 localizes to splicing factor-rich nuclear speckles and assembles transcription and splicing components into complexes through its amino and carboxyl regions. *Mol Cell Biol*, **26**, 4998-5014.

64 Zhou, Y., Zhou, B., Pache, L., Chang, M., Khodabakhshi, A.H., Tanaseichuk, O., Benner, C. and Chanda, S.K. (2019) Metascape provides a biologist-oriented resource for the analysis of systems-level datasets. *Nat Commun*, **10**, 1523.

65 Scully, R., Panday, A., Elango, R. and Willis, N.A. (2019) DNA double-strand break repair-pathway choice in somatic mammalian cells. *Nat Rev Mol Cell Biol*, **20**, 698-714.

66 Gottlieb, T.M. and Jackson, S.P. (1993) The DNA-dependent protein kinase: requirement for DNA ends and association with Ku antigen. *Cell*, **72**, 131-142.

67 Davis, A.J., Chen, B.P. and Chen, D.J. (2014) DNA-PK: a dynamic enzyme in a versatile DSB repair pathway. *DNA Repair (Amst)*, **17**, 21-29.

68 Lafont, F., Fleury, F. and Benhelli-Mokrani, H. (2020) DNA-PKcs Ser2056 auto-phosphorylation is affected by an O-GlcNAcylation/phosphorylation interplay. *Biochim Biophys Acta Gen Subj*, **1864**, 129705.

69 Cui, X., Yu, Y., Gupta, S., Cho, Y.M., Lees-Miller, S.P. and Meek, K. (2005) Autophosphorylation of DNA-dependent protein kinase regulates DNA end processing and may also alter double-strand break repair pathway choice. *Mol Cell Biol*, **25**, 10842-10852.

70 Sibanda, B.L., Chirgadze, D.Y., Ascher, D.B. and Blundell, T.L. (2017) DNA-PKcs structure suggests an allosteric mechanism modulating DNA double-strand break repair. *Science*, **355**, 520-524.

71 Liu, S., Shao, Y., Wang, Q., Zhai, Y. and Li, X. (2019) Genotoxic stress causes the accumulation of DNA-dependent protein kinase catalytic subunit phosphorylated at serine 2056 at nuclear speckles and alters pre-mRNA alternative splicing. *FEBS Open Bio*, **9**, 304-314.

72 Consortium, G.M.o.H.s.D., Lee, J.-M., McLean, Z.L., Correia, K., Shin, J.W., Lee, S., Jang, J.-H., Lee, Y., Kim, K.-H., Choi, D.E. *et al.* (2024) Genetic modifiers of somatic expansion and clinical phenotypes in Huntington's disease reveal shared and tissue-specific effects. *bioRxiv*, in press., 2024.2006.2010.597797.

73 Xu, H., Bensalel, J., Raju, S., Capobianco, E., Lu, M.L. and Wei, J. (2023) Characterization of huntingtin interactomes and their dynamic responses in living cells by proximity proteomics. *J Neurochem*, **164**, 512-528.

74 Hung, V., Udeshi, N.D., Lam, S.S., Loh, K.H., Cox, K.J., Pedram, K., Carr, S.A. and Ting, A.Y. (2016) Spatially resolved proteomic mapping in living cells with the engineered peroxidase APEX2. *Nat Protoc*, **11**, 456-475.

75 Liu, H., McCollum, A., Krishnaprakash, A., Ouyang, Y., Shi, T., Ratovitski, T., Jiang, M., Duan, W., Ross, C.A. and Jin, J. (2024) Roscovitine, a CDK Inhibitor, Reduced Neuronal Toxicity of mHTT by Targeting HTT Phosphorylation at S1181 and S1201 In Vitro. *Int J Mol Sci*, **25**.

76 Kegel, K.B., Meloni, A.R., Yi, Y., Kim, Y.J., Doyle, E., Cuiffo, B.G., Sapp, E., Wang, Y., Qin, Z.H., Chen, J.D. *et al.* (2002) Huntingtin is present in the nucleus, interacts with the transcriptional corepressor C-terminal binding protein, and represses transcription. *J Biol Chem*, **277**, 7466-7476.

77 Hung, C.L., Maiuri, T., Bowie, L.E., Gotesman, R., Son, S., Falcone, M., Giordano, J.V., Gillis, T., Mattis, V., Lau, T. *et al.* (2018) A patient-derived cellular model for Huntington's disease reveals phenotypes at clinically relevant CAG lengths. *Mol Biol Cell*, **29**, 2809-2820.

78 Yadav, M., Harding, R.J., Li, T., Xu, X., Gall-Duncan, T., Khan, M., Bardile, C.F., Sequiera, G.L., Duan, S., Chandrasekaran, R. *et al.* (2024) Huntingtin is an RNA binding protein and participates in NEAT1-mediated paraspeckles. *Sci Adv*, **10**, eado5264.

79 Chen, X., Xu, X., Chen, Y., Cheung, J.C., Wang, H., Jiang, J., de Val, N., Fox, T., Gellert, M. and Yang, W. (2021) Structure of an activated DNA-PK and its implications for NHEJ. *Mol Cell*, **81**, 801-810 e803.

80 Kurosawa, A. (2021) Autophosphorylation and Self-Activation of DNA-Dependent Protein Kinase. *Genes (Basel)*, **12**.

81 Raina, K. and Rao, B.J. (2022) Mammalian nuclear speckles exhibit stable association with chromatin: a biochemical study. *Nucleus*, **13**, 58-73.

82 Ilik, I.A. and Aktas, T. (2022) Nuclear speckles: dynamic hubs of gene expression regulation. *FEBS J*, **289**, 7234-7245.

83 Mintz, P.J., Patterson, S.D., Neuwald, A.F., Spahr, C.S. and Spector, D.L. (1999) Purification and biochemical characterization of interchromatin granule clusters. *EMBO J*, **18**, 4308-4320.

84 Shi, Y., Chen, J., Zeng, W.J., Li, M., Zhao, W., Zhang, X.D. and Yao, J. (2021) Formation of nuclear condensates by the Mediator complex subunit Med15 in mammalian cells. *BMC Biol*, **19**, 245.

85 Brahma, S. and Henikoff, S. (2024) The BAF chromatin remodeler synergizes with RNA polymerase II and transcription factors to evict nucleosomes. *Nat Genet*, **56**, 100-111.

86 Justice, J.L., Greco, T.M., Hutton, J.E., Reed, T.J., Mair, M.L., Botas, J. and Cristea, I.M. (2024) Multi-epitope immunocapture of huntingtin reveals striatum-selective molecular signatures. *bioRxiv*, in press., 2024.2009.2007.611843.

87 Peskett, T.R., Rau, F., O'Driscoll, J., Patani, R., Lowe, A.R. and Saibil, H.R. (2018) A Liquid to Solid Phase Transition Underlying Pathological Huntingtin Exon1 Aggregation. *Mol Cell*, **70**, 588-601 e586.

88 Kim, J., Han, K.Y., Khanna, N., Ha, T. and Belmont, A.S. (2019) Nuclear speckle fusion via long-range directional motion regulates speckle morphology after transcriptional inhibition. *J Cell Sci*, **132**.

89 Atwal, R.S., Xia, J., Pinchev, D., Taylor, J., Epand, R.M. and Truant, R. (2007) Huntingtin has a membrane association signal that can modulate huntingtin aggregation, nuclear entry and toxicity. *Hum Mol Genet*, **16**, 2600-2615.

90 Guccione, E. and Richard, S. (2019) The regulation, functions and clinical relevance of arginine methylation. *Nat Rev Mol Cell Biol*, **20**, 642-657.

91 Wu, Q., Schapira, M., Arrowsmith, C.H. and Barsyte-Lovejoy, D. (2021) Protein arginine methylation: from enigmatic functions to therapeutic targeting. *Nat Rev Drug Discov*, **20**, 509-530.

92 Burger, K., Ketley, R.F. and Gullerova, M. (2019) Beyond the Trinity of ATM, ATR, and DNA-PK: Multiple Kinases Shape the DNA Damage Response in Concert With RNA Metabolism. *Front Mol Biosci*, **6**, 61.

93 Giono, L.E., Nieto Moreno, N., Cambindo Botto, A.E., Dujardin, G., Munoz, M.J. and Kornblihtt, A.R. (2016) The RNA Response to DNA Damage. *J Mol Biol*, **428**, 2636-2651.

94 Aviner, R., Lee, T.T., Masto, V.B., Li, K.H., Andino, R. and Frydman, J. (2024) Polyglutamine-mediated ribotoxicity disrupts proteostasis and stress responses in Huntington's disease. *Nat Cell Biol*, **26**, 892-902.

95 Guo, Q., Bin, H., Cheng, J., Seefelder, M., Engler, T., Pfeifer, G., Oeckl, P., Otto, M., Moser, F., Maurer, M. *et al.* (2018) The cryo-electron microscopy structure of huntingtin. *Nature*, **555**, 117-120.

96 Herbrich, S.M., Cole, R.N., West, K.P., Jr., Schulze, K., Yager, J.D., Groopman, J.D., Christian, P., Wu, L., O'Meally, R.N., May, D.H. *et al.* (2013) Statistical inference from multiple iTRAQ experiments without using common reference standards. *J Proteome Res*, **12**, 594-604.

Figure Legends

Figure 1. Double Strand Break DNA damage response (DSB/DDR) is impaired in HD. A, DSB/DDR induction by bleomycin is measured by γ-H2A.X and p-ATM immunoblotting. B, Quantification of γH2A.X foci. Representative images (top panels) and 3D reconstruction (bottom panels, Imaris) of control and HD ISPNs stained with γ-H2A.X specific antibody upon induction of DSB by bleomycin, (10μg/ml, 30min), or from untreated cells (NT). C, graphs show 3D quantification. Data represent mean ±SEM. Two-sample t-tests with equal variances were performed. * $p<0.05$, n=5. DSB/DDR quantification shows lower γH2A.X foci size and intensity in HD ISPNs compared to normal ISPNs. D, HD ISPNs are more vulnerable to DSB-induced stress. Control (33CAG) and HD (180CAG) ISPNs were treated with 10μg/ml of bleomycin for indicated time and ATP and Casp3/7 levels were measured. Data is presented as mean % ± SEM of corresponding non-treated group. One-way ANOVA with Pairwise Multiple Comparison Procedures (Holm-Sidak method): *p=0.029, n=3; **p=0.001, n=3. T-test with equal variances: ^ $p<0.001$, n=3; ^^ p=0.004, n=3; ^^^ p=0.017, n=3

Figure 2. HTT phosphorylation at S1181 is modulated by the induction of DSB response. A, Relative quantification of phospho-serine S1181 by Parallel Reaction Monitoring (PRM) mass spectrometry. PRM measured abundances of AALPSLTNPPSLpSPIRR peptide from normal or polyQ-expanded mHTT proteins cut out from the HTT gel bands after immunoprecipitation from total cell lysates of control (33CAG) and HD (180CAG) ISPNs upon induction of DSB by bleomycin, (10μg/ml, 30min), or from untreated cells (NT). PRM data were analyzed with Skyline program. Graphs show peak area ratios to global standards grouped by condition. Statistical data

analysis was performed by Skyline program using triplicate samples for each cell line (n=3). *P<0.05. P value was adjusted for the multiple comparisons within this group. The adjustment was done using Benjamini-Hochberg procedure by Skyline program. B-C, pS1181 HTT is localized to nuclear puncta with increased size and intensity in HD ISPNs after induction of DSB. B, Representative images of normal and HD ISPNs treated with bleomycin (10µg/ml, 30min) co-stained with pS1181-HTT and γ-H2A.X specific antibodies. Nuclei were visualized with DAPI. C, 3D quantification (Imaris) of pS1181 HTT nuclear puncta. Data represent mean ±SEM. One-way ANOVA with Pairwise Multiple Comparison Procedures (Holm-Sidak method): * p<0.001, n=5.

Figure 3. Phospho-HTT co-localizes with nuclear speckle marker SC35. A, Representative images of ISPNs treated with bleomycin (10µg/ml, 30min) co-stained with pS1181-HTT and SC35 antibodies. Nuclei were visualized with DAPI. B, Orthogonal projections of Z-stacks demonstrate co-localization. C, 3D quantification (Imaris) of SC35-positive nuclear speckles (NS). Data represent mean ±SEM. One-way ANOVA with Pairwise Multiple Comparison Procedures (Holm-Sidak method): ** p<0.001, n=5; # p=0.002, n=5; ^ p=0.006, n=5

Figure 4. Unbiased screen for HTT interactors upon induction of DSB/DDR. A, PCA plots, B, Heat map and C, Volcano plot comparing protein abundances between HD and control samples after normalizing to HTT abundance (PD2.4). Green and pink boxed areas represent 20%- fold change (FC) at P <0.05. D, Pathway and process enrichment analysis of proteins decreased (HD/Cont <0.8) in abundance in HTT pulldowns from HD ISPNs relative to control ISPNs (generated using "Metascape" analysis tools (64). "Log10(P)" is the enrichment p-value in log base 10. E, Protein-protein Interaction (PPI) Enrichment Analysis generated by "Metacsape" of proteins decreased in abundance in HD ISPNs vs control neurons. Table shows best-scoring terms by p-value with functional description of the corresponding MCODE components.

Figure 5. HTT is phosphorylated by and co-localizes and interacts with DNA-PKcs. A, Quantitative channels values view (exported from PD2.41) for DNA-PKcs (PRKDC) showing grouped abundances from the pulldowns of control and HD ISPNs. B, Representative co-IP experiments from control (33) and HD (180) ISPNs treated with bleomycin (10µg/ml, 2h) and untreated (NT). Total cell lysates were prepared and HTT complexes were immuno-precipitated using antibodies to total HTT (MCA2050, two top panels). DNA-PKcs and HTT were detected in the immunoprecipitates (IPs). In reverse, DNA-PKcs protein was immunoprecipitated (two middle

panels) and phospho-HTT protein was detected in the eluates using a specific antibody to pS1181. The inputs for HTT, DNA-PKcs and beta-tubulin are shown below the IPs. C, *In vitro* phosphorylation assays with recombinant HTT-23Q/HAP40 complex. DNA-PK complex (Promega), activated by the addition of linear double-stranded DNA, was incubated with HTT/HAP40 for indicated times, and phosphorylation state of HTT was assessed using indicated phospho-specific antibodies. Graph shows quantitation of phospho-HTT normalized to total HTT. Data represent mean ±SEM. Mann-Whitney Rank Sum Test: *p=0.029, n=4. D, Representative images of normal (33CAG) and HD (180CAG) ISPNs treated with bleomycin (10µg/ml, 2 h) co-stained with pS1181-HTT and DNA-PKcs antibodies. E, Proximity Ligation Assay (PLA) of normal (33CAG) and HD (180CAG) ISPNs treated with bleomycin (10µg/ml, 2 h) and untreated using pS1181-HTT and DNA-PKcs antibodies.. Graphs show quantification of PLA signals using MetaXpress software (Molecular Devices). The data is presented as mean ±SEM of the number of nuclear PLA sites per cell, sum intensity of nuclear PLA sites per cell and average nuclear PLA site intensity relative to technical negative control within each experiment. 30-50 cells were analyzed for each condition. One-way ANOVA with Pairwise Multiple Comparison Procedures (Holm-Sidak method): ** $p<0.001$, n=5; # $p=0.004$, n=5.

Figure 6. Phosphorylated DNA-PKcs (S2056) associates with nuclear speckles and is decreased in HD cells. A, Levels of pDNA-PKcs (S2056) are decreased in HD ISPNs. Western blot with indicated antibodies of total cell lysates prepared from control (33) and HD (180) ISPNs treated with bleomycin (10µg/ml, 2h) and untreated (NT). Graph shows quantitation of phospho-DNA-PKcs normalized to total DNA-PKcs. Data represent mean ±SEM. Mann-Whitney Rank Sum Test: *p=0.02, n=3; **$p<0.001$. B, Representative images of ISPNs treated with bleomycin (10µg/ml, 2 h) co-stained with pDNA-PKcs (S2056) and SC35 antibodies. Orthogonal projections of z-stacks on right panels demonstrate co-localization.

Figure 7. Huntingtin (HTT) interacts with components of BAF chromatin remodeling complex. A, BAF chromatin remodeling and Mediator complexes identified among HTT-associated proteins (Metascape analysis). The schematics of BAF complex (middle panel) illustrates proteins found in HTT pulldowns indicated by red arrows. B, Representative co-IP experiments from control (33) and HD (180) ISPNs treated with bleomycin (10µg/ml, 2h) and untreated (NT). Total cell lysates were prepared and HTT complexes were immuno-precipitated using antibodies to total HTT (MCA2050). BRG1, ARID1A and HTT were detected in the

immunoprecipitates (IPs). IgG negative control IPs are shown at the bottom panels. The inputs for HTT, BRG1, ARID1A and beta-tubulin are shown (right panels).

Figure 8. HTT /BRG1 (SMARCA4) co-localization and direct interaction in ISPNs A, Representative images of ISPNs treated with bleomycin (10µg/ml, 2 h) co-stained with BRG1 and HTT (MCA2050) antibodies. Orthogonal projections of Z-stacks (shown for red and green merged panels) demonstrate co-localization. B, Proximity Ligation Assay (PLA) in normal (33CAG) and HD (180CAG) ISPNs treated with bleomycin (10µg/ml, 2 h) and untreated using BRG1 and HTT antibodies. Images shown for 180 ISPNs were taken at higher intensity for illustrative purpose, while quantitation was done with the same settings as for 33 ISPNs. Graphs show quantification of PLA signals using MetaXpress software (Molecular Devices). The data is presented as mean ±SEM of the number of nuclear PLA sites per cell, sum intensity of nuclear PLA sites per cell and average nuclear PLA site intensity relative to technical negative control within each experiment. 30-50 cells were analyzed for each condition. T-test with equal variances: *p=0.016, n=4; ** p=0.011, n=4; ***p=0.009, n=4; #p=0.005, n=4; ##p<0.001, n=4; ^p=0.006, n=4; ^^p=0.002, n=4.

Figure 9. HTT /ARID1A co-localization and direct interaction in ISPNs A, Representative images of ISPNs treated with bleomycin (10µg/ml, 2 h) co-stained with ARID1A and HTT (MCA2050) antibodies. Orthogonal projections of Z-stacks (shown for red and green merged panels) demonstrate co-localization. B, Proximity Ligation Assay (PLA) in normal (33CAG) and HD (180CAG) ISPNs treated with bleomycin (10µg/ml, 2 h) and untreated using ARID1A and HTT antibodies. Images shown for 180 ISPNs were taken at higher intensity for illustrative purpose, while quantitation was done with the same settings as for 33 ISPNs. Graphs show quantification of PLA signals using MetaXpress software (Molecular Devices). The data is presented as mean ±SEM of the number of nuclear PLA sites per cell, sum intensity of nuclear PLA sites per cell and average nuclear PLA site intensity relative to technical negative control within each experiment. 30-50 cells were analyzed for each condition. *One-way ANOVA with Pairwise Multiple Comparison Procedures (Holm-Sidak method): p<0.001, n=4; ^ T-test with equal variances. P<0.001, n=4; ^^ Mann-Whitney Rank Sum Test. P=0.029, n=4.

Figure 10. APEX2-mediated proximity labeling for HTT interactions. A, Pathway and process enrichment analysis of proteins found in proximity of HTT with at least one biotinylated (biotin-tyramide) peptide (generated using “Metascape” analysis tools ,Zhou et al. 2019). “Log10(P)” is the enrichment p-value in log base 10. E, Protein-protein Interaction (PPI) Enrichment Analysis

generated by “Metacsape” of the same database as in A. Table shows best-scoring terms by p-value with functional description of the corresponding MCODE components.

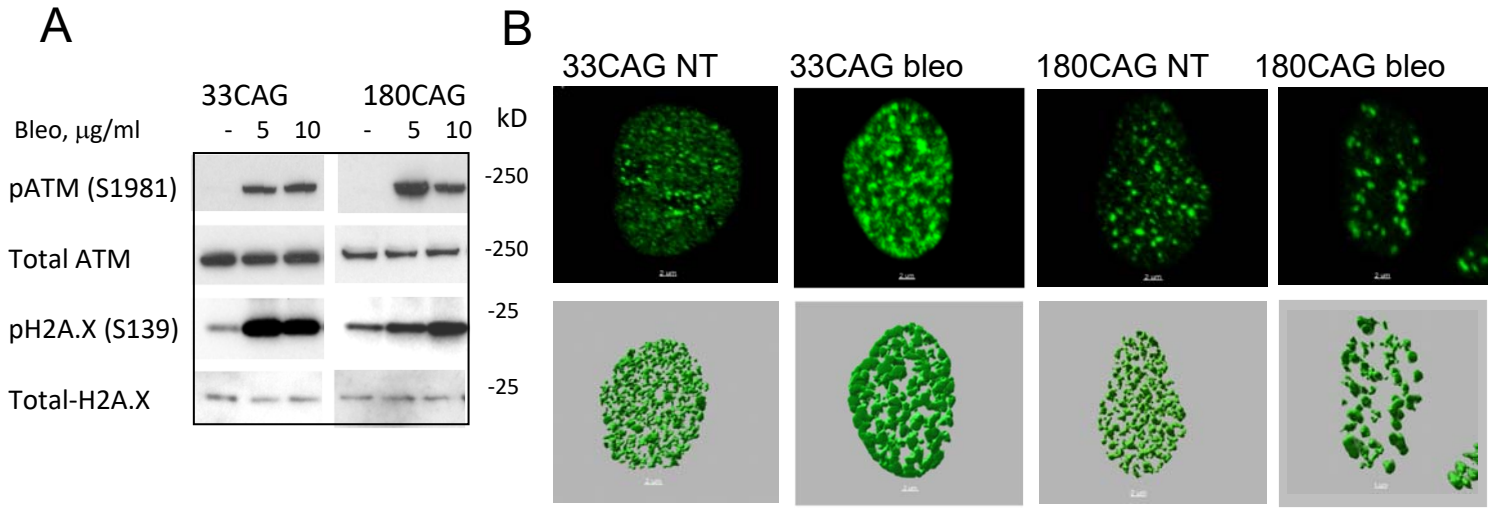

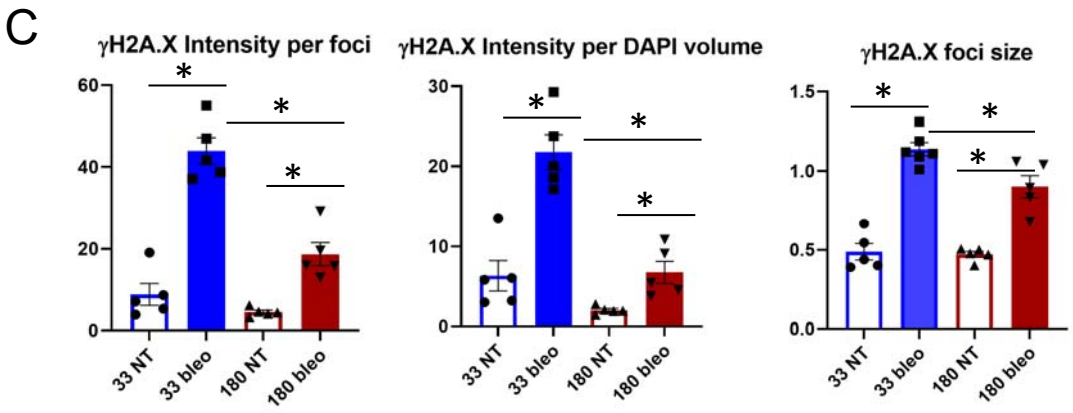

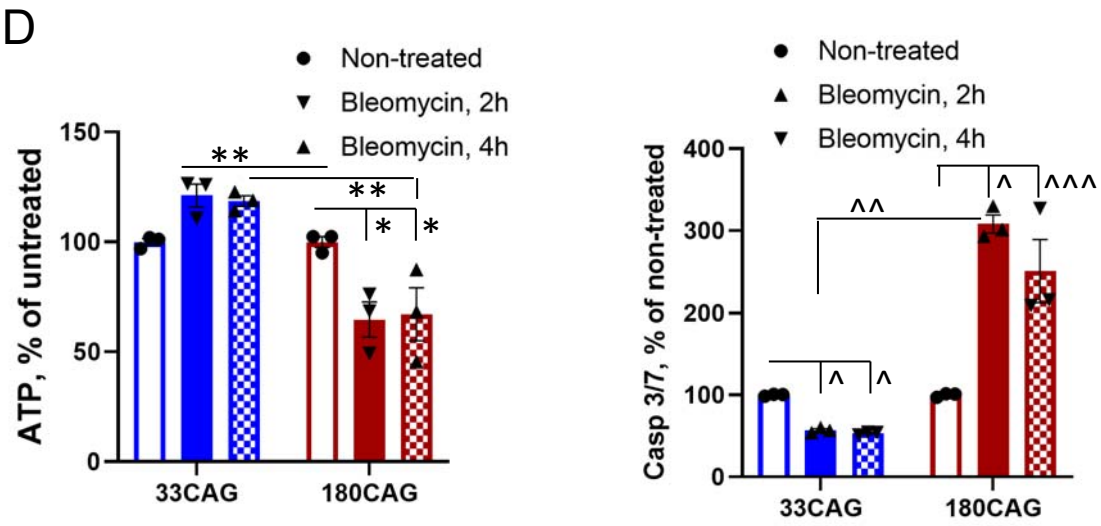

Figure 1

A

Peak area ratios to global standards grouped by condition

S1181-phospho AALPSLTNPPSLSPIRR

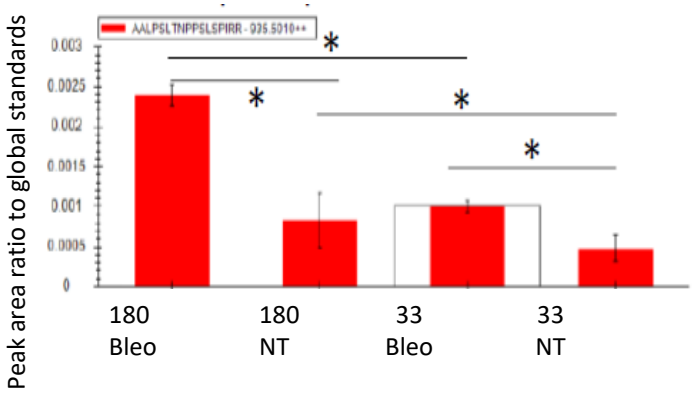

Transitions of precursors and product ions

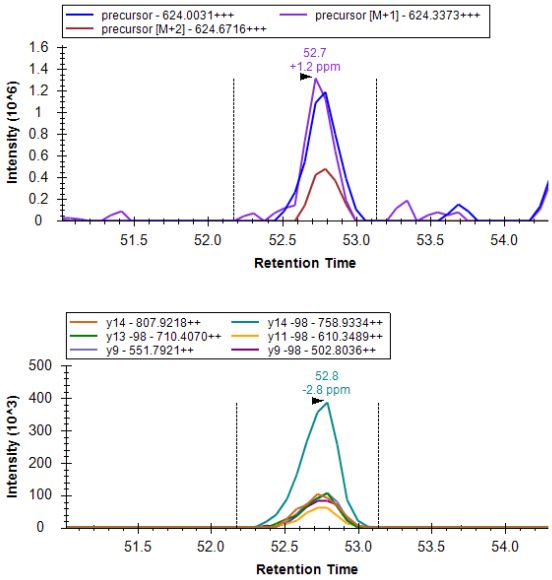

B

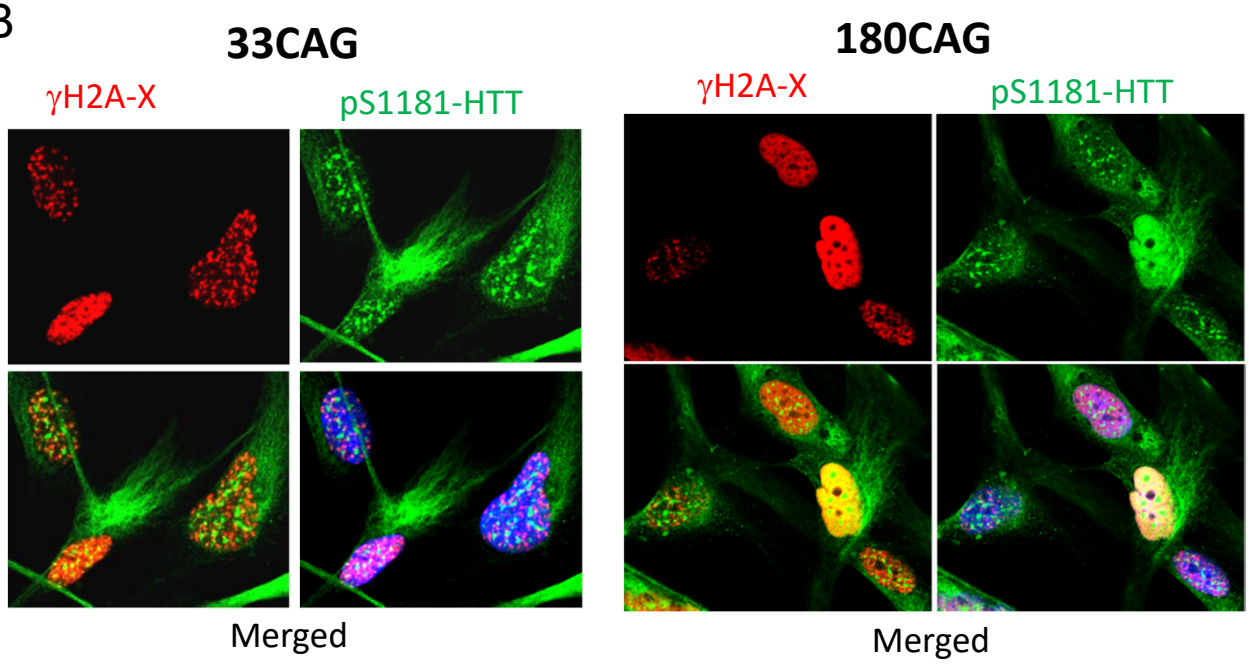

C

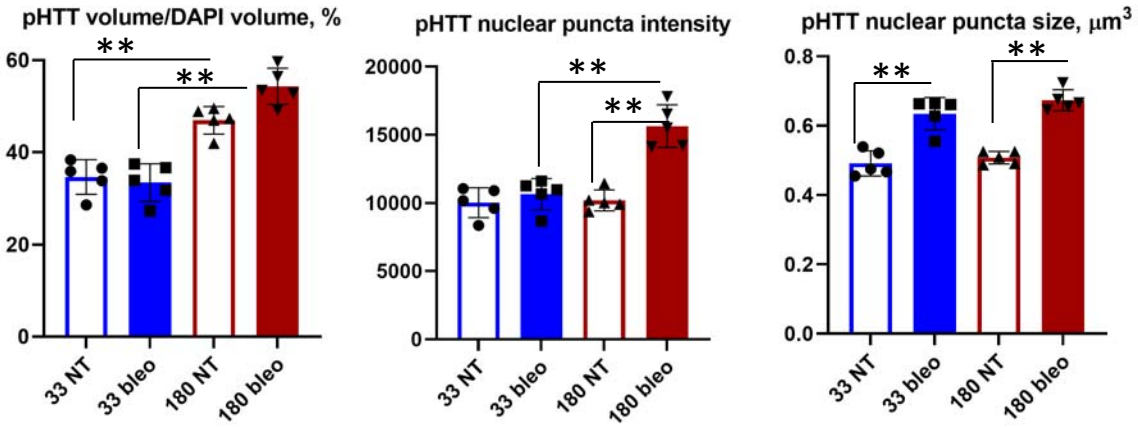

Figure 2

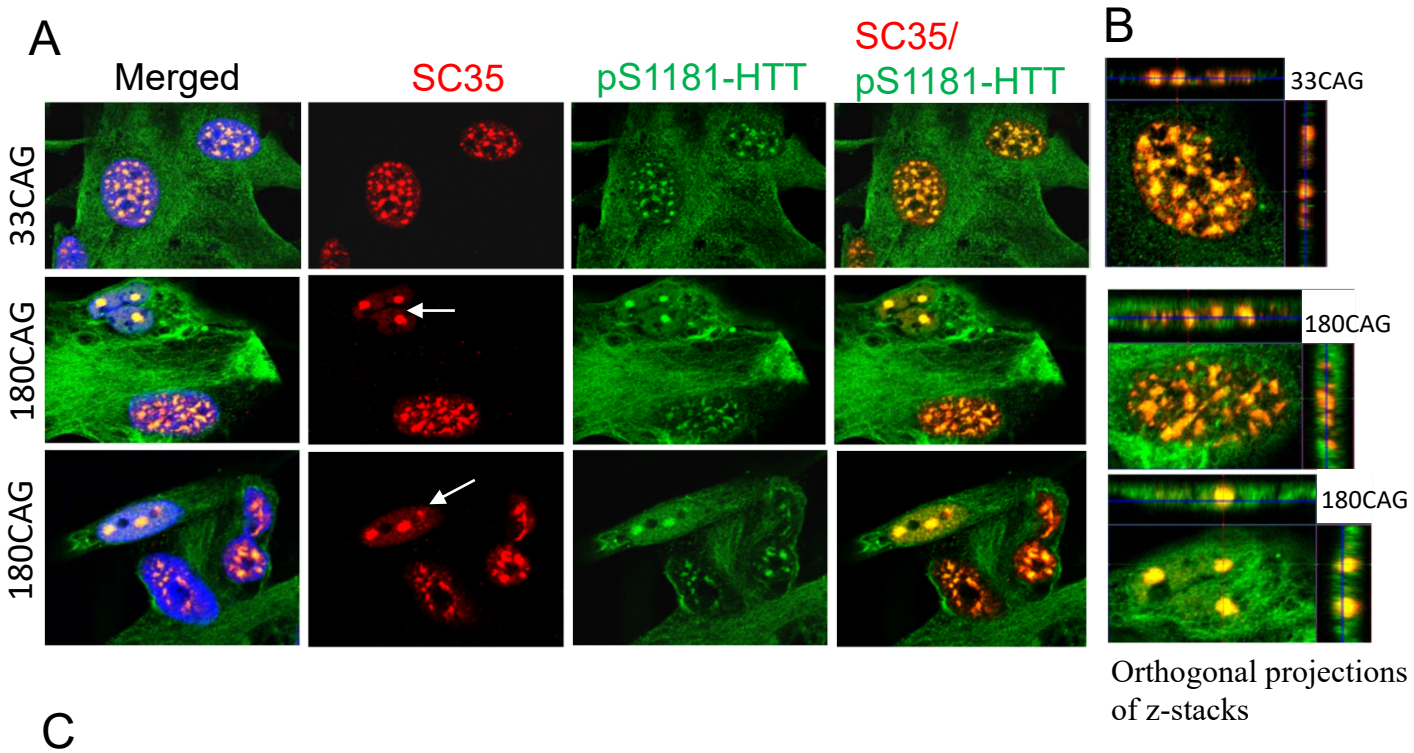

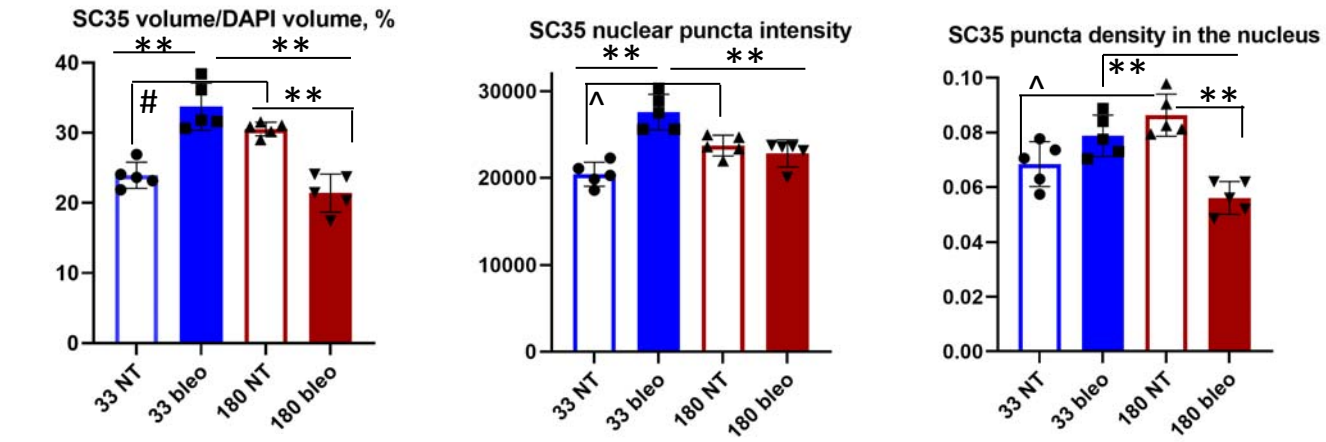

Figure 3

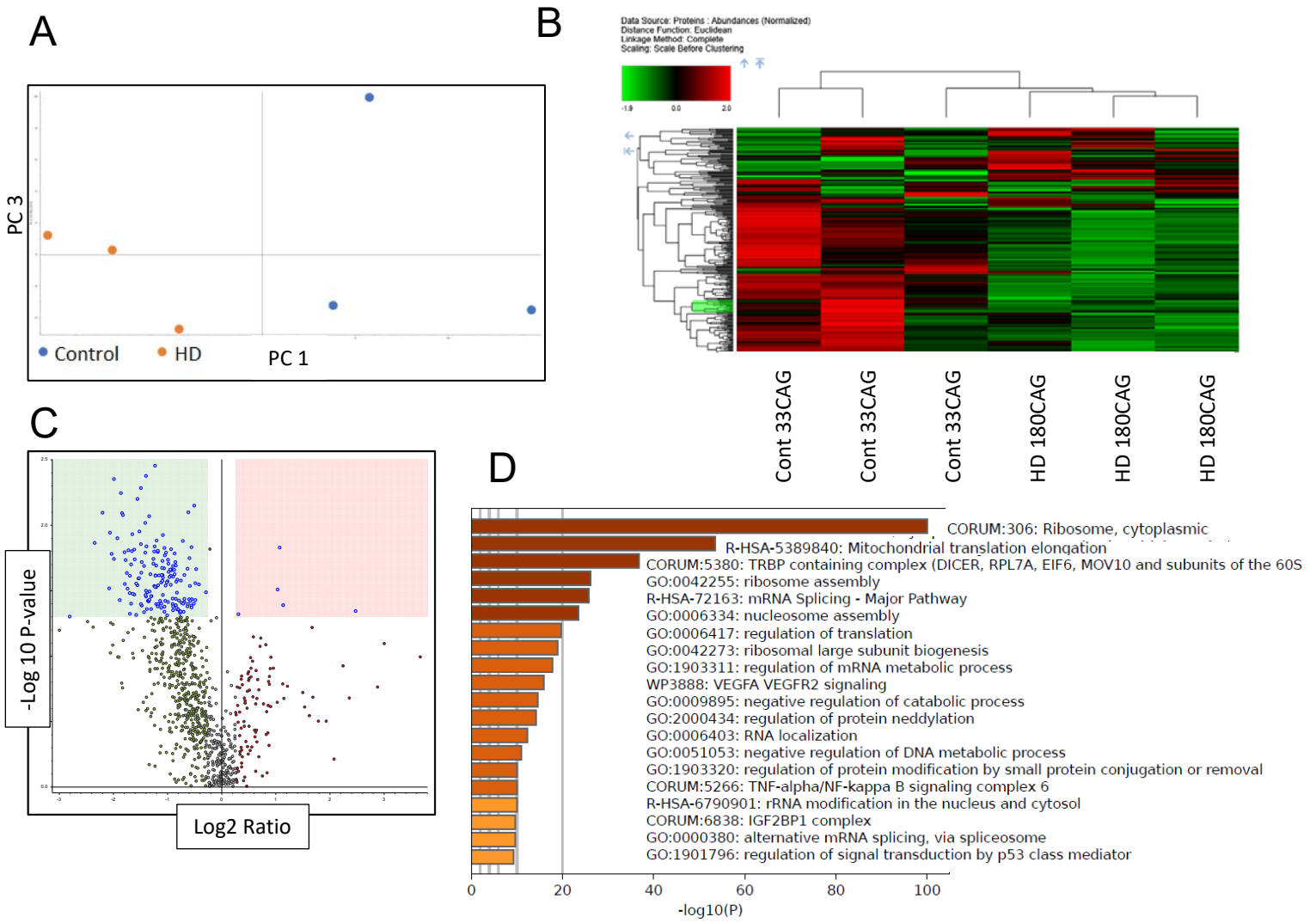

MCODE	Color	GO	Description	Log10(P)
MCODE_1		CORUM:306	Ribosome, cytoplasmic	-100.0
MCODE_1		R-HSA-156902	Peptide chain elongation	-100.0
MCODE_2		R-HSA-5419276	Mitochondrial translation	-56.8
MCODE_3		R-HSA-72163	mRNA Splicing - Major Pathway	-14.9
MCODE_4		GO:0061644	protein localization to CENP-A chromatin	-37.0
MCODE_5		R-HSA-8953854	Metabolism of RNA	-11.0
MCODE_5		GO:0006417	regulation of translation	-10.8

Figure 4

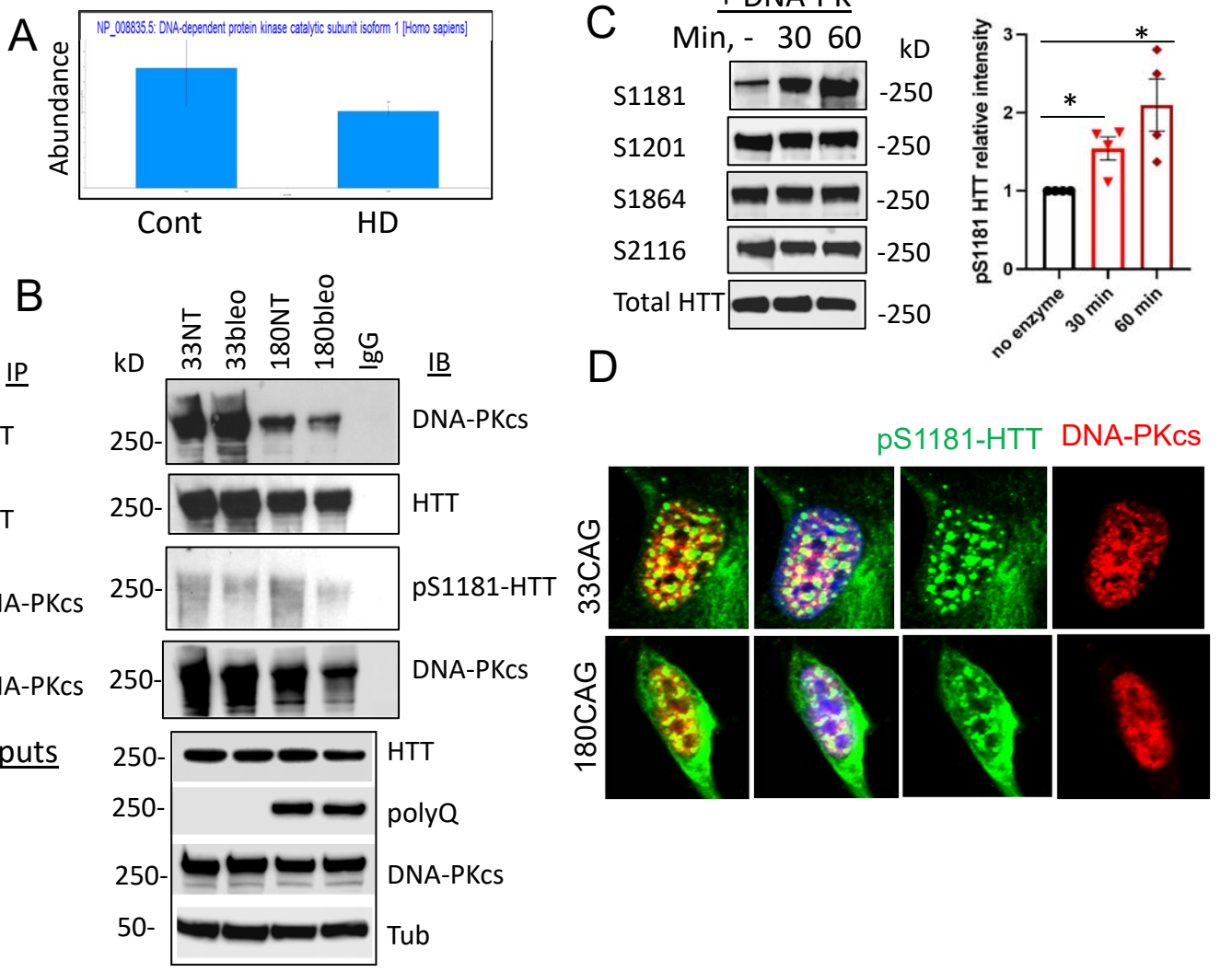

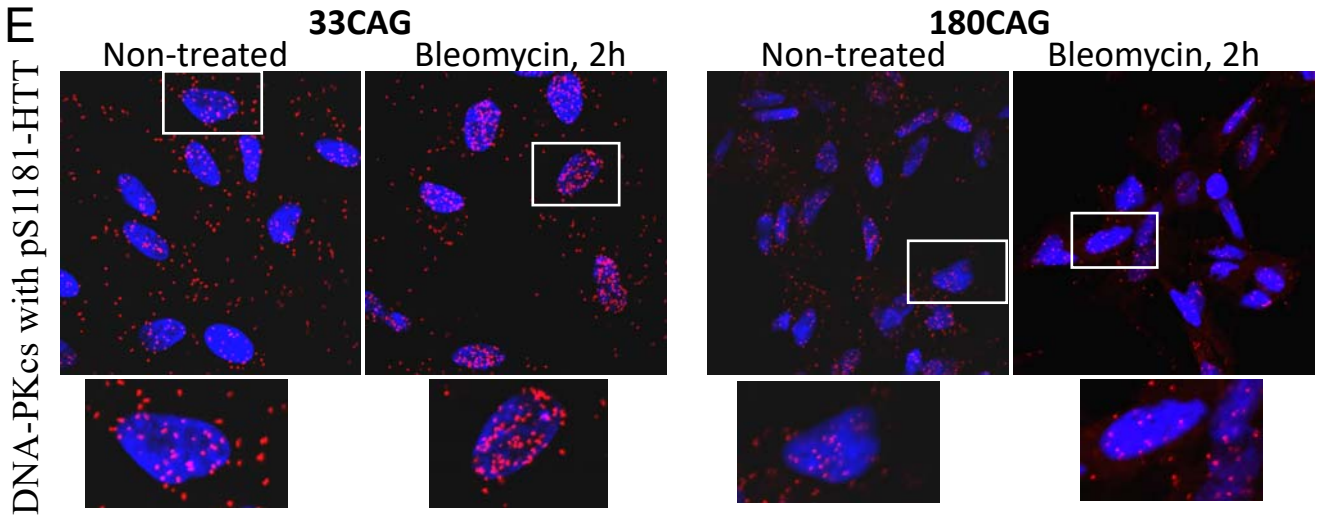

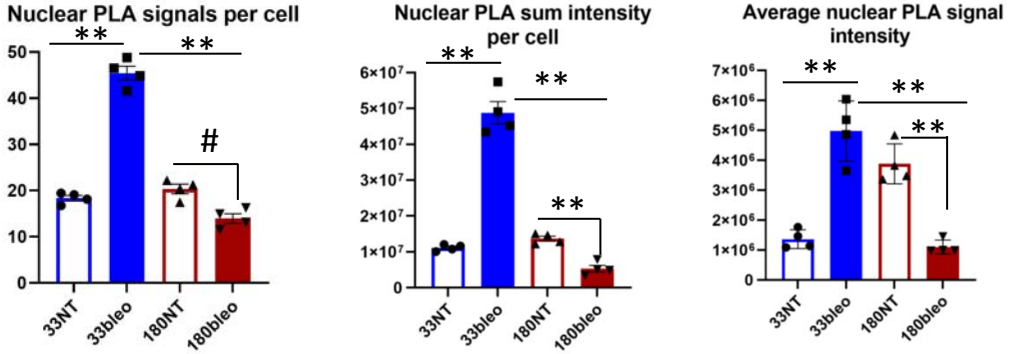

Figure 5

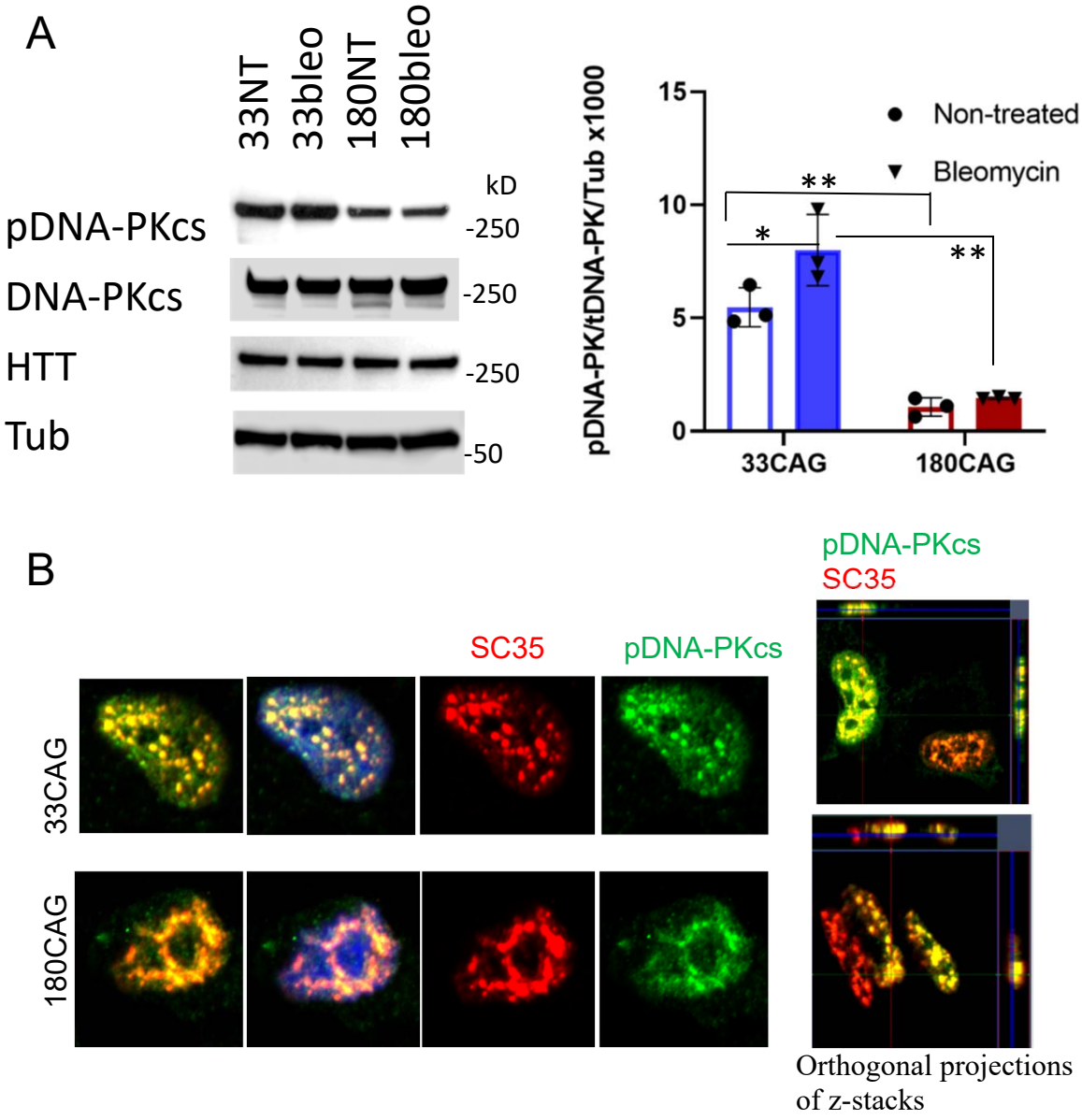

Figure 6

A

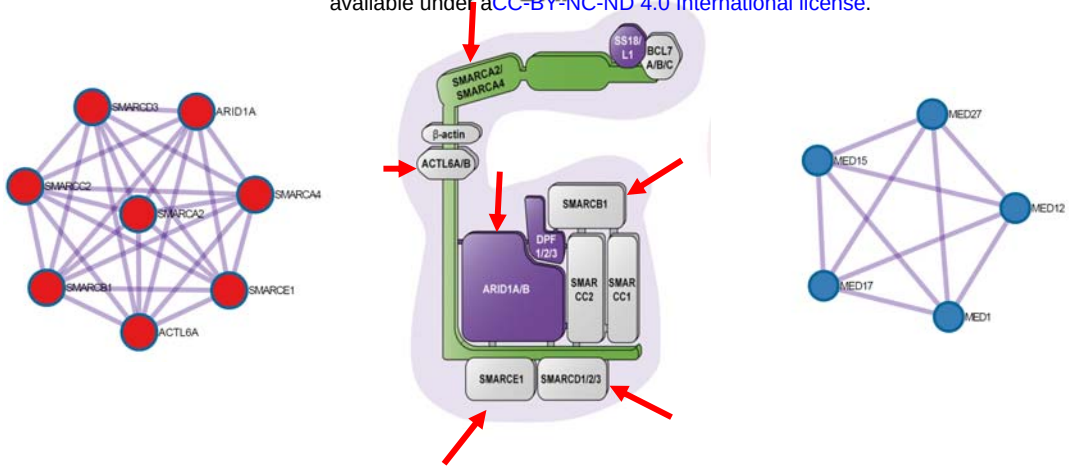

MCODE	Color	GO	Description	Log10(P)
MCODE_1		CORUM:1237	BAF complex	-25.2
MCODE_1		GO:2000819	regulation of nucleotide-excision repair	-24.8
MCODE_1		CORUM:238	SWI-SNF chromatin remodeling-related-BRCA1 complex	-24.7
MCODE_2		CORUM:230	Mediator complex	-15.0
MCODE_2		GO:0060261	positive regulation of transcription initiation by RNA polymerase II	-13.5
MCODE_2		GO:2000144	positive regulation of DNA-templated transcription initiation	-13.3

B

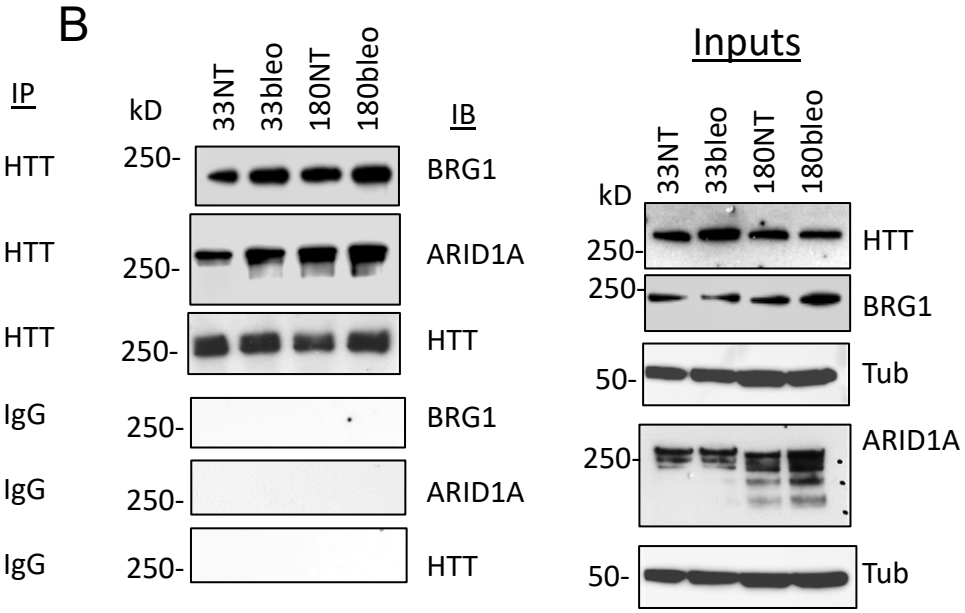

Figure 7

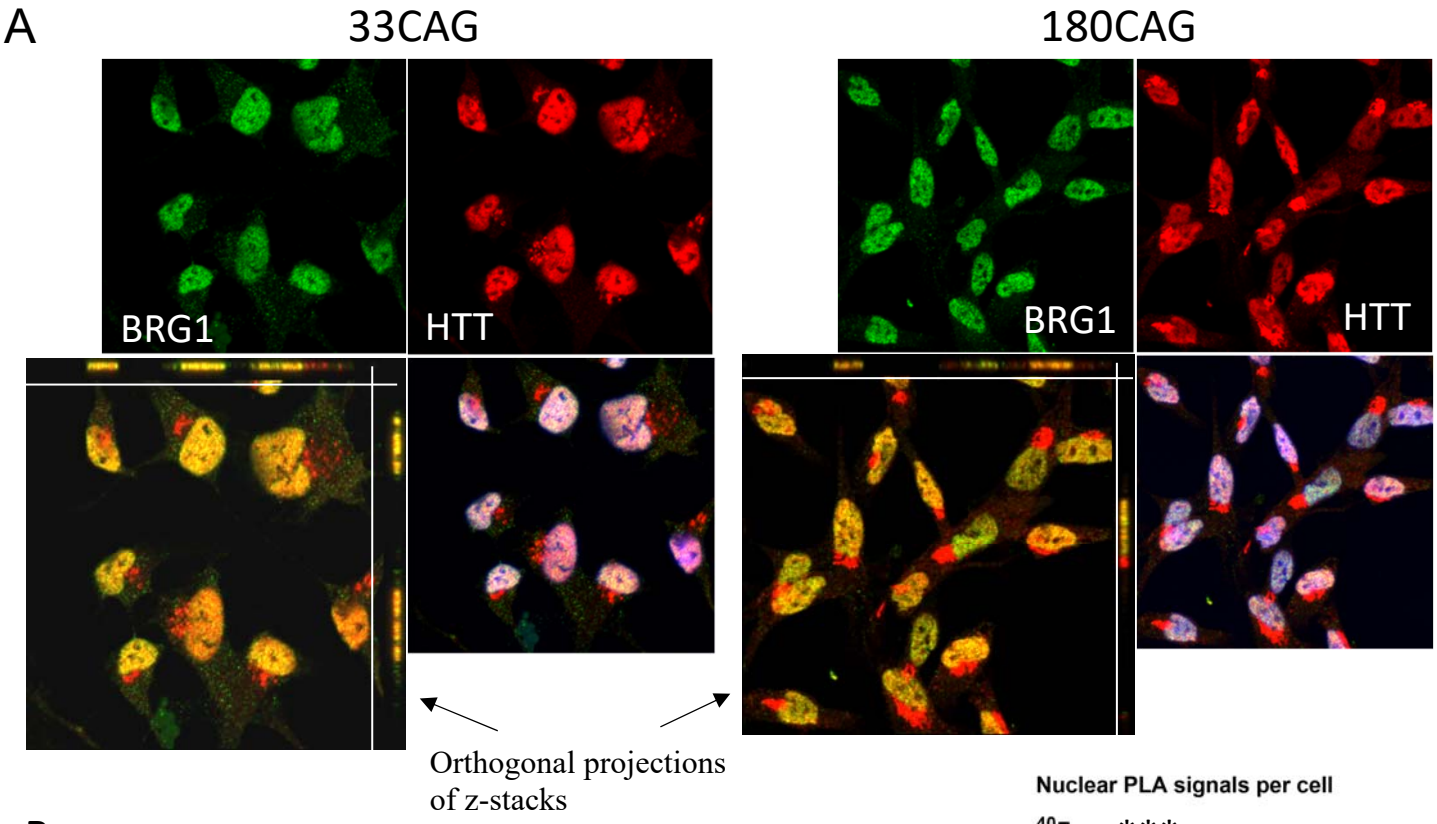

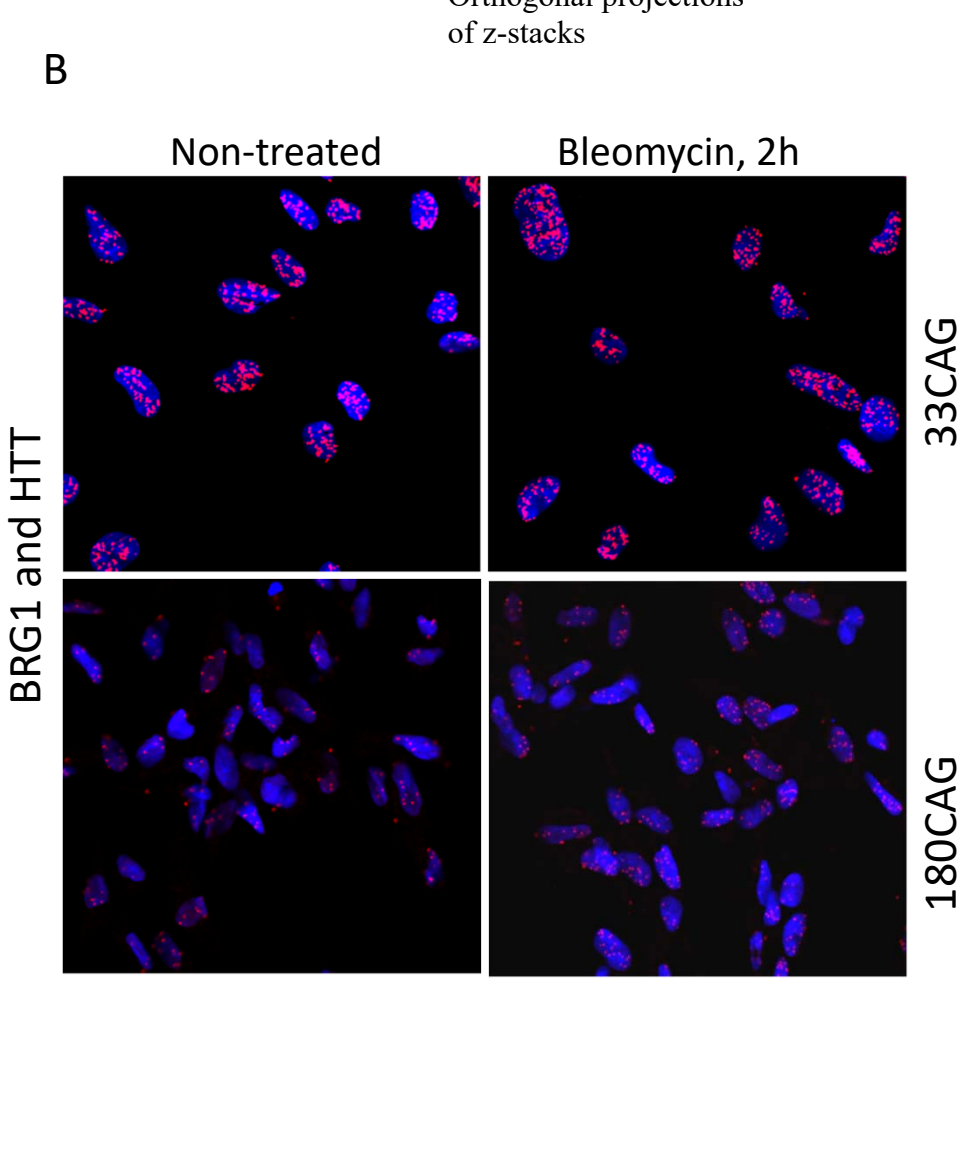

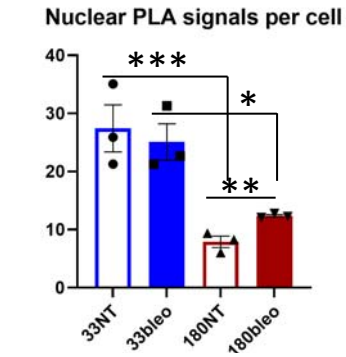

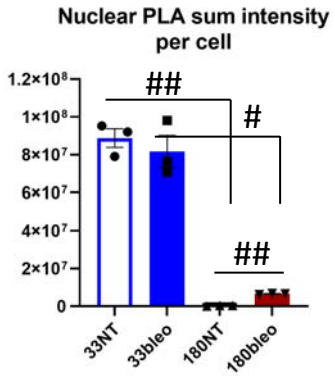

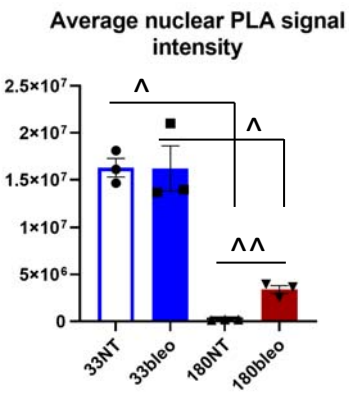

Figure 8

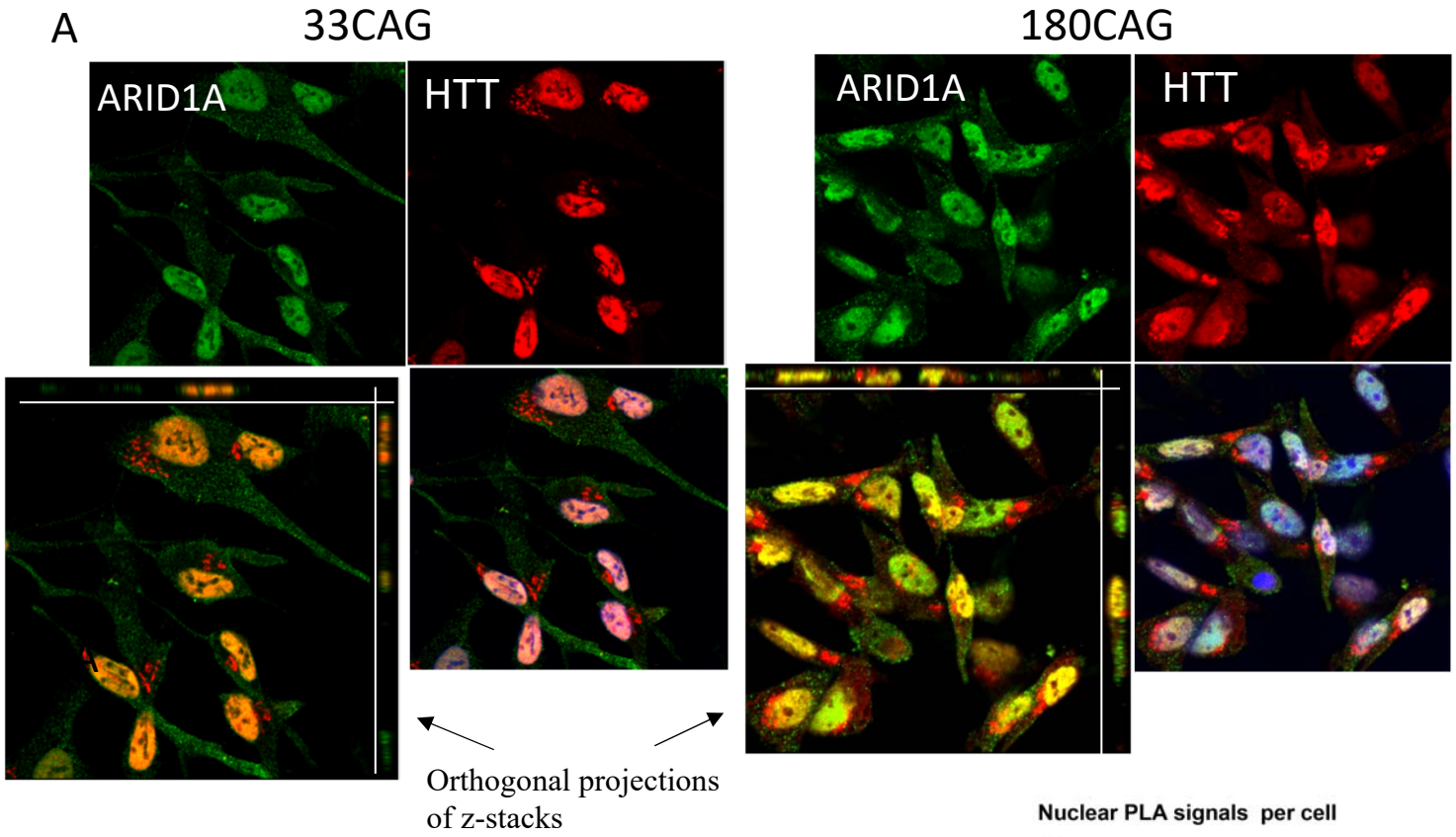

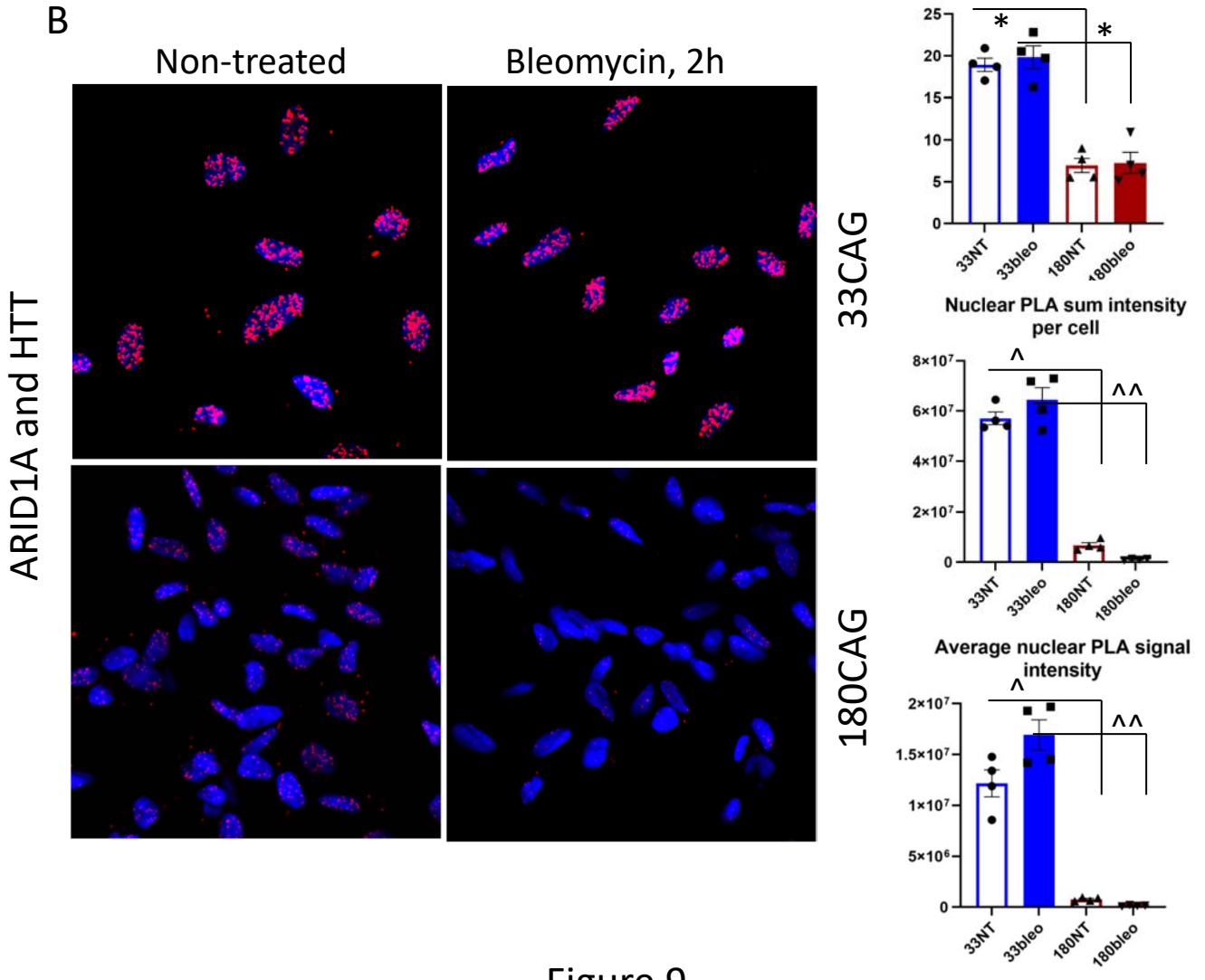

Figure 9

A

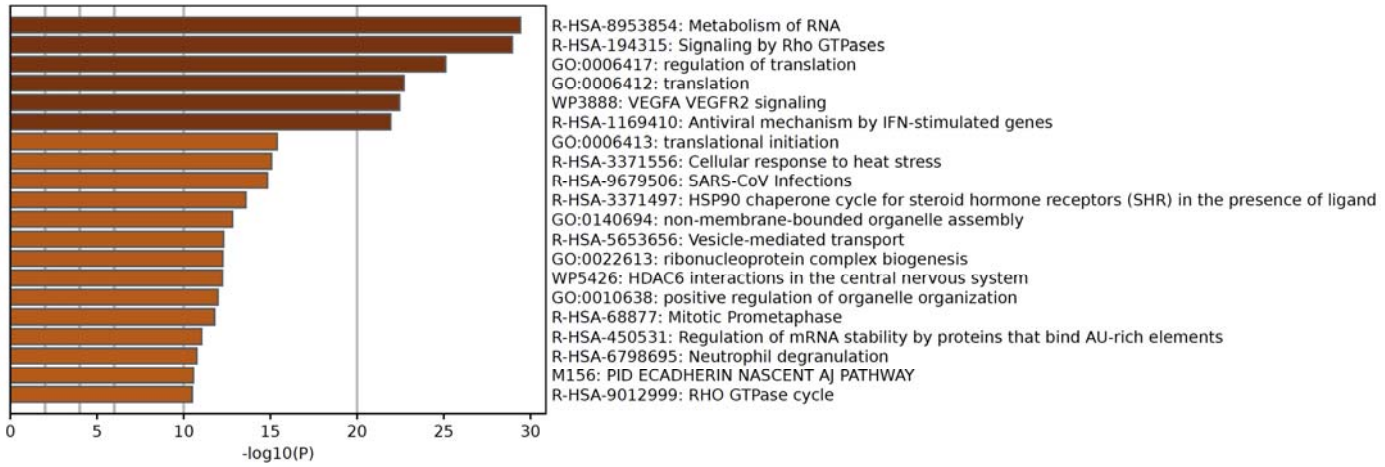

B

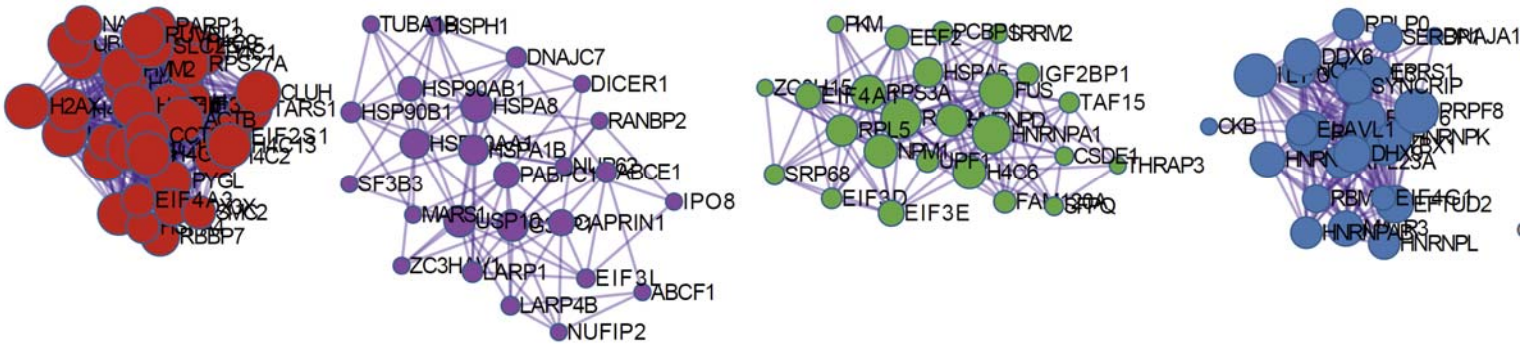

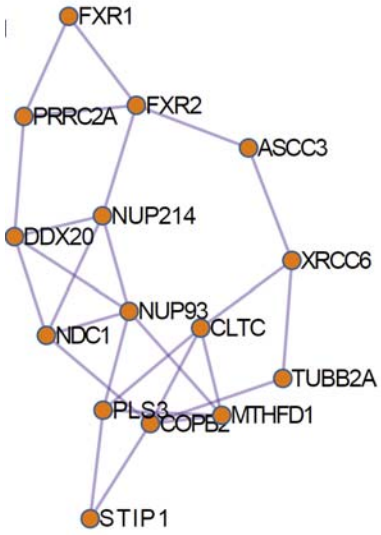

Color	GO	Description	Log10(P)
MCODE_1	GO:0061644	protein localization to chromatin	-35.2
MCODE_1	GO:0071168	protein localization to chromatin	-32.9
MCODE_2	R-HSA-8953854	Metabolism of RNA	-21.7
MCODE_2	WP411	mRNA processing	-15.3
MCODE_2	GO:1903311	regulation of mRNA metabolic process	-14.1
MCODE_3	GO:0045727	positive regulation of translation	-15.1
MCODE_3	GO:0034250	positive regulation of amide metabolism	-14.3
MCODE_3	GO:1903312	negative regulation of mRNA metabolism	-11.9
MCODE_4	R-HSA-3371556	Cellular response to heat stress	-14.4
MCODE_4	GO:0006457	protein folding	-11.2
MCODE_4	R-HSA-3371453	Regulation of HSF1- heat shock response	-10.7
MCODE_5	GO:0051028	mRNA transport	-8.5
MCODE_5	GO:0050657	nucleic acid transport	-8.1
MCODE_5	GO:0050658	RNA transport	-8.1

Figure 10